

THE UNIVERSITY OF NEW SOUTH WALES



SCHOOL OF ELECTRICAL ENGINEERING
AND TELECOMMUNICATION

Augmentation of Inverter Control System to Implement Inertia Emulation

by

Matthew Davis

Thesis submitted as a requirement for the degree
Bachelor of Engineering (Electrical Engineering)

Submitted: October 27, 2016

Supervisor: John Fletcher

Abstract

The rotational inertia of the turbines in conventional generators (such as gas and coal) helps stabilise the frequency of the electricity grid. Batteries and most renewable generation sources do not exhibit such inertial behaviour. Therefore grids with high penetration levels of renewables and batteries will have large and rapid frequency deviations, which is undesirable.

Inverters can be programmed to independently and autonomously mimic the inertial behaviour of conventional generators, thereby contributing inertial support to the grid even though they lack moving parts. For batteries such functionality has been simulated but not experimentally verified.

In this thesis droop control and inertia emulation were added to the control system of a programmable inverter. Experimental testing confirmed that this functionality successfully controls the output power to closely match the behaviour of a system with real inertia. The reaction time of this new control system is 200 ms, which is fast enough to be useful during most credible contingencies in the Australian grid. The system developed in this thesis works sufficiently well, and will help address frequency regulation issues in the high-renewables, low inertia grids of the future.

Acknowledgements

I would like to thank Professor John Fletcher for his assistance throughout the year. He was always willing to spend time to help me.

Contents

I	Introduction	1
I.1	Background	1
I.2	Aim	1
I.3	Design	1
I.4	Simulations	2
I.5	Experiments	2
I.6	Document Structure	2
II	Literature Review	4
II.1	Network Frequency Dynamics	4
II.1.1	Inertia	4
II.1.2	Load Relief	6
II.1.3	Frequency Response	7
II.1.4	Current Methodology	9
II.1.5	Industry Challenges	9
II.1.6	Proposed Solution	11
II.1.6.1	Variable Speed Wind Turbines	11
II.1.6.2	Storage	12
II.1.6.3	Commercial Incentives	13
II.2	Inverters	13
II.2.1	Switching	13
II.2.2	Filtering	14
II.2.3	Control	14
III	Problem Statement	15
III.1	Context	15
III.2	Goal	15
IV	Design	16
IV.1	Constraints	16
IV.2	Control Architecture	16
IV.3	Droop	17

IV.4	Inertia	20
IV.5	Frequency Measurement	22
IV.6	Filtering	23
IV.6.1	Motivation and General Requirements	23
IV.6.2	Frequency Filter	23
IV.6.3	Frequency Derivative Mean	24
IV.7	Power Setpoint Saturation	25
V	Simulations	26
V.1	Motivation	26
V.2	Switching Model	26
V.3	Limitations	28
V.4	Verification of Experimental Approach	28
VI	Experimental Setup	31
VI.1	Overview	31
VI.2	Inverter	33
VI.3	Grid Simulator	33
VI.4	DC Supply	33
VI.5	Power Analyser	33
VI.6	Protection and Isolation	34
VI.7	Test Conditions	34
VII	Experimental Results	35
VII.1	Simple Frequency Deviation	35
VII.1.1	Frequency Waveform	35
VII.1.2	Droop Control	35
VII.1.3	Inertia Emulation	37
VII.2	Realistic Frequency Deviation	40
VII.2.1	Frequency Waveform	40
VII.2.2	Impact of Droop and Inertia	40
VII.3	Inertia Emulation Speed	43

VII.4	Directional Inertia	43
VIII Discussion		46
VIII.1	Results Summary	46
VIII.2	Polarity	46
VIII.3	Upper Inertia Limit	47
VIII.4	Speed of Inertial Response	47
VIII.4.1	Issue	47
VIII.4.2	Causes	47
VIII.4.3	Requirements	48
VIII.5	Directional Inertia	48
VIII.6	Commercial Value and Industry Significance	49
IX Conclusion		50
IX.1	Results	50
IX.2	Key Contributions	50
IX.3	Future Work	51
Bibliography		52
Appendices		55
Appendix A	Data Points For Frequency Deviations	55
Appendix B	Further Results	56
B.1	Realistic Over-frequency Deviation	56
B.2	Saturation	59

List of Figures

1	Scales analogy for imbalance between generation and load	5
2	Change in energy of a synchronous machine for a given change in rotational speed	6
3	Droop characteristics for two different droop settings	7
4	Network equilibrium point change for step increase in demand	8
5	Transient behaviour for step increase in demand	10
6	Typical three phase, two level inverter	14
7	Common inverter output filters	14
8	Current control calculation architecture	17
9	Pre-existing inverter control system	18
10	Inverter control system with inertia and droop added	19
11	PLL Design	22
12	IIR Filter Structure	24
13	Improvements to average voltage source approximation for three phase inverter	27
14	Average switching model for the DC side	28
15	Simulation results confirming the effect of droop and virtual inertia on grid frequency	30
16	Schematic of experimental setup	31
17	Photographs of equipment used in experimental setup	32
18	Experimental results for simple frequency deviations for all 3 settings	36
19	Comparison of experimental results to ideal during simple frequency deviations with droop and without inertia	37
20	Comparison of experimental results to ideal during simple frequency deviations with inertia and without droop	38
21	Comparison of experimental results to ideal during simple frequency deviations with droop and inertia	39
22	Experimental results for a realistic under frequency deviation for all 3 settings	41
23	Comparison of experimental results to ideal during realistic under frequency deviation with droop and inertia	42
24	Overall propagation delay and rise time of inertial response	44
25	Comparison of normal and directional inertia	45
26	Experimental results for a realistic over frequency deviation for all 3 settings	57
27	Comparison of experimental results to ideal during realistic over frequency deviations with droop and inertia	58
28	Demonstration of control system saturation	59

List of Tables

1	Logic for inertia contribution with directional inertia	21
2	Data points for simple frequency deviation	55
3	Data points for realistic frequency deviation	55

Acronyms

AC alternating current

AEMO The Australian Energy Market Operator

DC direct current

DSP digital signal processor

FCAS frequency control ancillary services

FIR finite impulse response

IGBT insulated gate bipolar transistor

IIR infinite impulse response

NEM National Electricity Market

PI proportional and integral

PLL phase locked loop

PR proportional-resonant

PV photovoltaic

PWM pulse width modulation

RAM random access memory

RMS root mean squared

ROCOF rate of change of frequency

VSM virtual synchronous machine

Part I

Introduction

I.1 Background

The output of all generators in the electricity grid should match the total load at all times. During normal operation there is a slight mismatch between the two, and after network events (such as a generator tripping out) there is a large mismatch. The difference between the two is met by drawing from or adding to the kinetic energy of all spinning masses connected to the grid, such as the turbines of coal and gas generators. This change in kinetic energy results in a change in electrical frequency. A higher amount of inertia results in a slower change in frequency for a given mismatch between generation and load. This means that after a network event the frequency will have deviated less by the time generation reacts to the event to correct the mismatch. Consequently the inertia of the turbines in conventional generators helps stabilise the frequency of the electricity grid.

Batteries and photovoltaics (PV) have no moving parts, and hence no inertia. Wind turbines do have physical inertia, but the inertia in modern variable speed turbines is decoupled from the grid, so they do not provide inertial support. Therefore in a modern grid with high levels of PV, wind and batteries, there will be low levels of inertia, which will result in large and rapid frequency deviations, which will threaten grid stability. Since grids with high levels of renewables are crucial in the fight against climate change, addressing the issue of low inertia is important.

The inverters in batteries and other devices can be programmed to emulate the inertial behaviour of synchronous machines, thereby providing inertial support to the grid even though the device lacks moving parts. An inverter and energy source with such functionality is called a virtual synchronous machine (VSM). Such a system would be able to operate autonomously, using only measurements from onboard frequency instrumentation, thereby eliminating the need for any communication infrastructure to a central dispatch centre.

I.2 Aim

The literature review shows that although there have been several simulations of battery based VSMs, there has not yet been any experimental verification to confirm that they function as intended. The aim of this thesis is to construct and experimentally test a battery based VSM, to confirm that battery systems can provide the same useful frequency support as conventional generators, despite lacking any moving parts.

I.3 Design

A 5 kVA, 3 phase, two level inverter was programmed to act as a VSM. A power control loop was added to the pre-existing C code to adjust the setpoint for the inner current control loop, to make the real power output equal to

- a nominal power setpoint;
- minus an amount proportional to the deviation of grid frequency from 50 Hz (droop control);
- minus an amount proportional to the time derivative of frequency (inertia emulation).

The code for this power control loop must execute within $30\ \mu\text{s}$. Consequently most of the code was written in fixed point, with the number of fractional bits adjusted throughout the system in order to maximise accuracy.

The pre-existing phase locked loop (PLL) did not meet the unique and stringent performance requirements necessary for a smooth yet fast inertial response. The PLL design described by Phipps et al. was implemented, with parameters which were co-optimised with subsequent filtering [1].

An innovative ‘directional’ inertia was conceived and implemented. This entails disabling inertia emulation when frequency is returning towards the nominal value, in order to hasten the return.

I.4 Simulations

A Simulink model of the inverter was developed for development and analysis purposes. The model utilises the exact C code and hardware used in the experimental testing. This was to ensure accuracy of the simulation (particularly with respect to fixed point operations), and to reduce the simulation time of the model.

The average switching model described by Paquette was further developed to model saturation more accurately [2]. Improvements to this model also include simulating the direct current (DC) side of inverter switching, including soft charging at startup.

A microgrid with an inverter and synchronous generator was simulated to confirm that if an inverter can control its output power as described above, then the inverter will help reduce the magnitude and speed of frequency deviations.

I.5 Experiments

An inverter with the aforementioned functionality was connected to a DC supply, and a programmable alternating current (AC) supply which can reproduce frequency deviations. The inverter’s output power during these deviations was measured, to confirm that the inverter can closely mimic the behaviour of conventional droop controlled generators with real inertia.

I.6 Document Structure

- Part II on page 4 contains the literature review, which explores the problem, the context and VSMs in greater detail.
- Part III on page 15 states the full aim of this thesis, the scope, and the motivation for this aim.
- Part IV on page 16 details the the design process, including the constraints, mathematical derivations and design considerations.

- Part V on page 26 documents the development of an accurate and fast simulation model of the specific inverter used, using the exact C code which is run on the inverter's processor in the experimental testing. Section V.4 demonstrates through simulation of a microgrid that if the inverter's power output matches the intended output, then the inverter will successfully help reduce the speed and magnitude of grid frequency deviations.
- Part VI on page 31 states and justifies the experimental approach and setup used to verify the operation of the VSM. It includes details of the settings, test conditions and test equipment.
- Part VII on page 35 contains the results for the experimental testing, which demonstrate the successful operation of droop control and inertia emulation.
- Part VIII on page 46 discusses the limitations of the experimental results and VSMs more generally, and further explores issues discovered during the design and experimentation stages. Section VIII.6 on page 49 details the commercial value of the system implemented in this thesis, and the significance of it with respect to the Australian electricity industry.

Part II

Literature Review

II.1 Network Frequency Dynamics

Australia's electricity networks operate at a nominal frequency of 50 Hz. Other countries typically operate at either 50 Hz or 60 Hz. Many generators and loads are designed to operate only within a narrow band around the nominal frequency. Large deviations from the nominal frequency can result in maloperation and damage to equipment. Similarly many machines on the network cannot cope with fast rates of change of frequency. Consequently the minimisation of the magnitude and speed of frequency deviations is a critical objective of electricity network operation.

II.1.1 Inertia

Electricity grids need to be operated such that the amount of power produced by generators precisely equals the amount of power consumed by loads (plus losses) at all times. However no control system is perfect, and there will normally be a small mismatch between supply and demand. Immediately after network faults there can be a large mismatch between the two. In accordance with the Law of Conservation of Energy, this difference in energy must go to or come from somewhere. The source and sink of this energy is the combined kinetic energy of all synchronous machines connected to the network.

When there is more generation than load, the excess energy is automatically and instantaneously spent accelerating generator turbines, and motors. The rate of increase in kinetic energy is equal to the excess generation. A turbine's kinetic energy is proportional to its rotational speed squared. The rotational speed of a synchronous machine is proportional to electric frequency. Consequently the electrical frequency of the electricity network increases when there is more generation than load. The inverse happens when there is less generation than load. Figure 1 shows an analogy for this. When load and generation are not equal, the scales tip and frequency changes. Generation adjusts in response to this tipping, to restore the balance.

When generation matches load, the frequency of the network remains constant [3]. In Figure 1 this corresponds to balanced scales. The frequency changes if and only if the load does not match the generation. The rate of change of frequency (ROCOF) for a given mismatch is inversely proportional to the sum of the inertia of all spinning metal linked to the grid [4]. In the analogy in Figure 1, low inertia corresponds to a longer beam, resulting in faster scale tipping for the same imbalance. In this way the physical inertia of loads and generators directly correlates to the stability of an electricity network [5]. Low levels of inertia place the stability of the network at risk, whereas high levels of inertia slow down frequency deviations which makes frequency regulation easier [4, 6].

The most significant sources of inertia in a typical electricity network are the large metal turbines in coal, gas and nuclear power plants. Some loads also contribute to total system inertia, particularly industrial motors [7]. Devices without spinning parts such as PV arrays, batteries and many loads do not have inertia [4]. Modern variable speed wind turbines have power electronics interfaces which decouple the speed of the blades from the network frequency. So despite having a spinning turbine

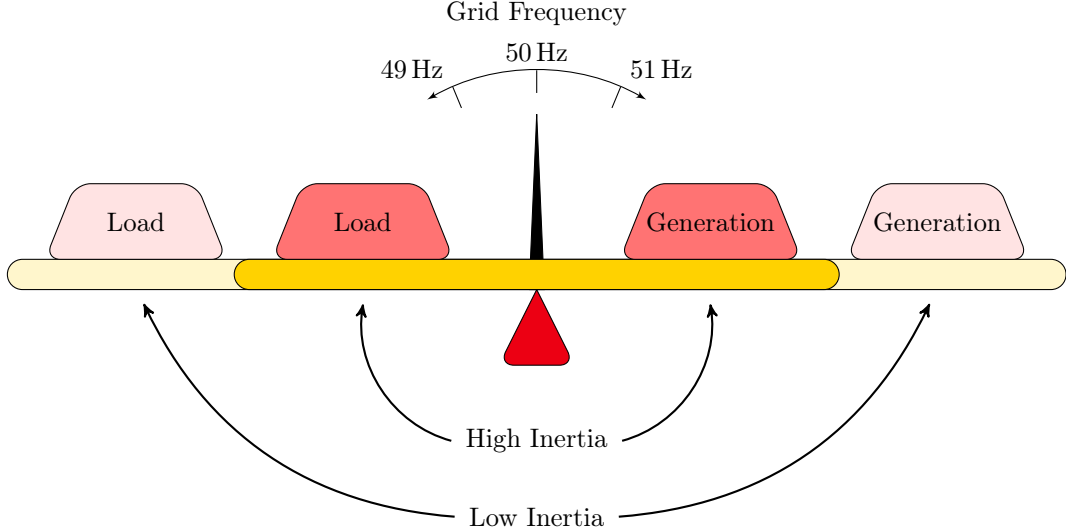


Figure 1: Scales analogy for imbalance between generation and load. When there is more or less generation than load, frequency begins increasing or decreasing respectively. In this analogy, low levels of inertia correspond to a longer beam, for which the same imbalance would cause faster scale tipping.

they do not provide noticeable inertial support to the network [6, 7, 8]. Older style fixed speed wind turbines lack a power electronics interface, so they do contribute inertia.

The amount of energy E stored in a spinning mass is given by

$$E = \frac{1}{2} J \omega_m^2 \quad (1)$$

where J is the rotational inertia and ω_m is the rotational speed [9]. In a single generator network, if the cumulative energy difference between generation and consumption over a given time is ΔE , then the machine speed will change by

$$\Delta E = \frac{1}{2} J \omega_{m_{\text{old}}}^2 - \frac{1}{2} J \omega_{m_{\text{new}}}^2 \quad (2)$$

This is shown graphically in Figure 2. If the mismatch is allowed to continue indefinitely the frequency will tend towards zero or infinity, and the network will become unstable and collapse. Typically the mismatch is small, and averages out to zero over minutes.

The transient response for small deviations from nominal is given by

$$M_m \omega_m \frac{d^2 \omega_m}{dt^2} - D_m \omega_m = P_m - P_e = \Delta P \quad (3)$$

where M_m is the angular momentum of the rotor at synchronous speed, D_m is the *damping coefficient*, P_m is the mechanical power from the shaft, and P_e is the electrical power leaving the generator terminals [3]. Equation 3 is known as the *swing equation*.

For networks with multiple machines, the electrical frequency must remain consistent across the network, therefore the percentage change in rotational frequency of each machine is the same.

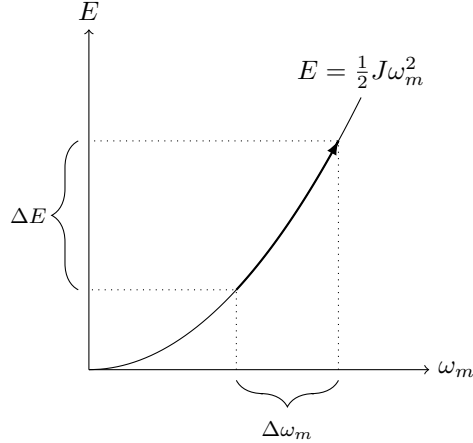


Figure 2: Change in the kinetic energy (ΔE) of a synchronous machine for a given change in rotational speed ($\Delta \omega_m$).

A convenient metric for comparing inertia between different generators is the *inertia constant* H , which is defined as the stored kinetic energy at nominal frequency ($\omega_{m,nom}$) divided by the generator's nameplate power rating¹ S_n [4].

$$H = \frac{\frac{1}{2}J\omega_{m,nom}^2}{S_n} \quad (4)$$

The intuitive meaning of H is the number of seconds it would take to slow down the machine to a halt by extracting kinetic energy at a rate equal to full power, without any injection of power from the prime mover [4]. Typical values of H are between 2 s and 10 s. Generators with larger nameplate capacities tend to have smaller inertia constants [11]. The inertia constant of wind turbines is comparable to that of conventional generators [8, 9].

II.1.2 Load Relief

For some types of loads the power drawn from the network is a function of network frequency. When the network frequency is above nominal, these loads consume more power than normal. When the network frequency is below nominal, these loads consume less power than nominal. For small deviations of frequency this relationship is approximately linear.

$$\frac{\Delta P_L}{P_L} \approx K_L \frac{\Delta f}{f_n} \quad (5)$$

Where P_L is the load power, f is the network frequency, f_n is the nominal frequency, and K_L is the *frequency sensitivity coefficient*, which is typically between 0.5 and 3 when averaged over the whole network [3].

Network frequency drops below nominal if and only if there is more load than generation. When this happens, the effect of load relief is that less power is drawn from the network, thereby reducing the mismatch between generation and load. In this way load relief automatically assists with frequency regulation, without any operator intervention.

¹For fixed speed wind turbines apparent power is used instead of nameplate capacity [10].

II.1.3 Frequency Response

To ensure the stability of each generator and of the network, governors act on generator turbines to produce a power frequency relationship such that frequency increases are responded to with power decreases, and frequency decreases are responded to with power increases [3]. This is known as a *droop characteristic* [9]. For small deviations this relationship is approximately linear, and is given by

$$D_{pf} = \frac{-\frac{\Delta f}{f_n}}{\frac{\Delta P}{P_n}} \quad (6)$$

where D_{pf} is the dimensionless *droop constant*, Δf is the change in frequency, f_n is the nominal frequency, ΔP is the change in power and P_n is the nominal power. Equation 6 is shown graphically in Figure 3, where curve A has more droop than curve B.

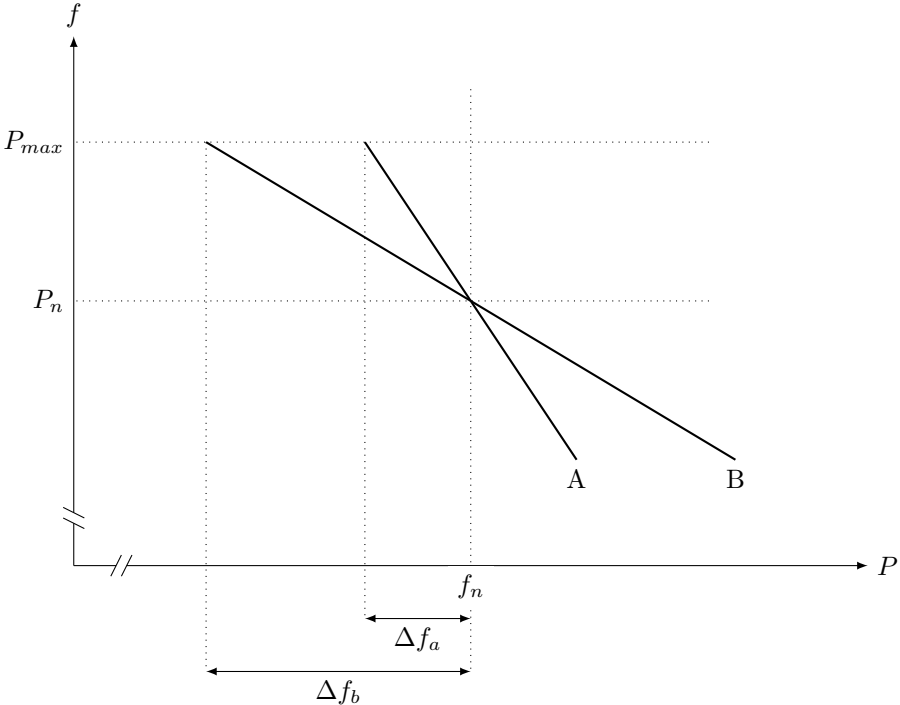


Figure 3: Droop characteristics for two different droop settings [9]. Curve A has more droop than curve B. P is output real power, f is frequency, and P_n is the nominal real power setpoint.

Droop complements load relief, in that they both help contribute to frequency regulation. However such frequency sensitivity of generators is due to active governor action, whereas load relief is an inherent and passive characteristic of some loads. Typically droop is far more significant than load relief [3].

The equilibrium point for a network is the intersection of the load and generator characteristic curves on the power-frequency plane. This is because generators and loads operate at the same frequency, and at equilibrium the power generated equals the power consumed. The change in equilibrium point in response to a step increase in load of ΔP_{demand} is shown in Figure 4. Prior to the step, the network is operating at point 1 in Figure 4, with frequency f_1 equal to nominal. The horizontal positioning of the initial generation characteristic curve of the generator (*Old Generation*) is determined by the setpoint

of the generators. The slope of the generator curve is determined by the amount of droop. The slope of the load curve is determined by the *frequency sensitivity coefficient* of the overall network, which is a measure of the amount of load relief. The horizontal positioning of the load curve is determined by the nominal amount of load.

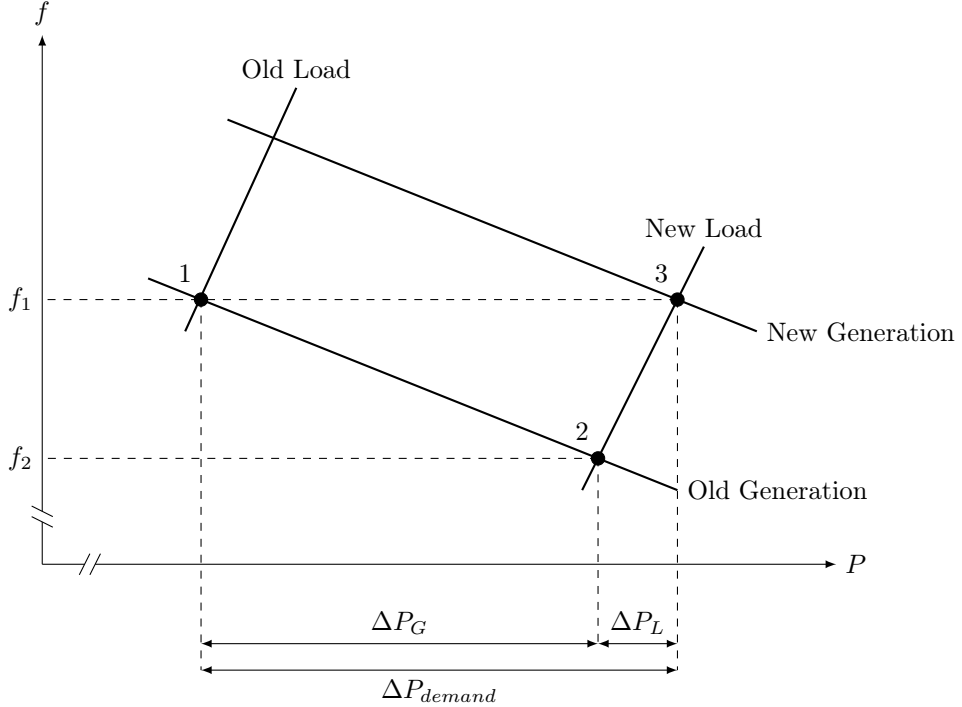


Figure 4: Network equilibrium point change for step increase in demand of ΔP_{demand} . The equilibrium moves from point 1 to 2, and frequency drops from f_1 to f_2 . The frequency change causes an increase in generation ΔP_G due to droop, and a decrease in load ΔP_L due to load relief. Secondary action then shifts the generation curve, bringing the equilibrium to point 3.

Immediately after the step from the old load to the new load there is a large imbalance between generator output and load consumption. The kinetic energy of all rotating turbines on the network is automatically and immediately drawn upon to meet this new demand. As a result of this reduction in kinetic energy, the frequency of the turbines drops, and hence the frequency of the network drops. This stage is called the *inertial response*. Due to load relief, total demand decreases as frequency falls. Due to generator governor action total generation output increases as frequency falls. A new equilibrium point forms at node 2 in Figure 4, when the increase in generator output ΔP_G (due to governor action), plus the reduction in load ΔP_L (due to load relief) equals the initial step increase in load ΔP_{demand} . Several seconds after the initial step (or less), the network temporarily settles upon node 2. This stage is called *primary control*. Upon detecting the drop in frequency, generators allocated to regulation support increase their generation setpoint to bring the network frequency back from f_2 to f_1 . On the power-frequency plane in Figure 4 this corresponds to the new generation characteristic curve, which is above the old one. After several minutes the network reaches the new equilibrium point at node 3, which is the intersection of the new load characteristic curve and the new generation characteristic curve. This stage is called *secondary control*.

The governors responsible for the generators' power-frequency curve are not ideal, so they have some lag. Consequently the path taken from node 1 to node 2 in Figure 4 is not a straight line. Due to the

lag, the operating point initially drops below the generator curve, and eventually oscillates around node 2. This is shown in Figure 5a [3]. After briefly settling on node 2, secondary control slowly moves the operating point to node 3. Since this latter transition is much slower, it is approximately along a straight line in Figure 5a. Figures 5b and 5d show the network frequency during this transient.

Figure 5c shows the oscillations in the power output of the generators during the transient, and of the load consumption. The area between the two curves is the mismatch in supply and demand. The difference in frequency between node 1 and node 2 is proportional to the area between the two curves up to point 2 in Figure 5c, as described by Equation 2 on page 5. Once the frequency has been restored to the initial value through secondary control (point 3), the total area between the two curves in Figure 5c will be zero.

Similar behaviour occurs for a step increase in load, or a step in generation.

II.1.4 Current Methodology

In the National Electricity Market (NEM) frequency regulation is achieved through the frequency control ancillary services (FCAS) markets, which are operated by The Australian Energy Market Operator (AEMO) [12]. One of the constraints placed upon dispatch is ensuring that there is sufficient primary control reserve. Primary control is enabled within 6 seconds of a frequency deviation through *fast raise* and *fast lower* services. Secondary control is achieved through the *slow raise*, *slow lower*, *delayed raise* and *delayed lower* services. These services begin within 5 minutes of a fault. After 5 minutes economic dispatch is used to adapt to a change.

A crude yet effective way of arresting downwards frequency deviations is under frequency load shedding. This involves deliberately disconnecting large blocks of load, to reduce the mismatch between generation and load. Under frequency load shedding is typically automated and implemented through local frequency sensors. Due to the detrimental impact of under frequency load shedding on customers it is used as a last resort. In grids with high penetrations of distributed generation, under frequency load shedding also disconnects generation sources, which cancels out some of the impact of the load shedding [13].

In Australia, AS 4777 specifies that all small scale inverters must reduce their output during over frequency events exceeding 50.25 Hz, ramping down to 0 W by 52 Hz [14]. Similarly all distributed generation with storage must ramp down consumption when charging during under frequency events below 49.75 Hz, ramping down to 0 W by 49 Hz. Similar requirements exist elsewhere in the world [11].

II.1.5 Industry Challenges

As mentioned in Section II.1.1, high levels of inertia make the network more stable, and make frequency regulation easier. Over the past few decades there has been an increase in PV and wind power which has displaced conventional generators. Since PV and modern wind turbines contribute no inertia to the network, this displacement is causing a decrease in the level of inertia in the electricity network. Over the coming decades as the penetration level of renewables increases further, the amount of inertia in the network will continue to decrease [7]. Furthermore, since an increasing portion of spinning loads are being connected with power electronics interfaces, the inertia contribution from loads is also decreasing. Similarly if pumped hydro storage is displaced by battery and fuel cell storage, total inertia

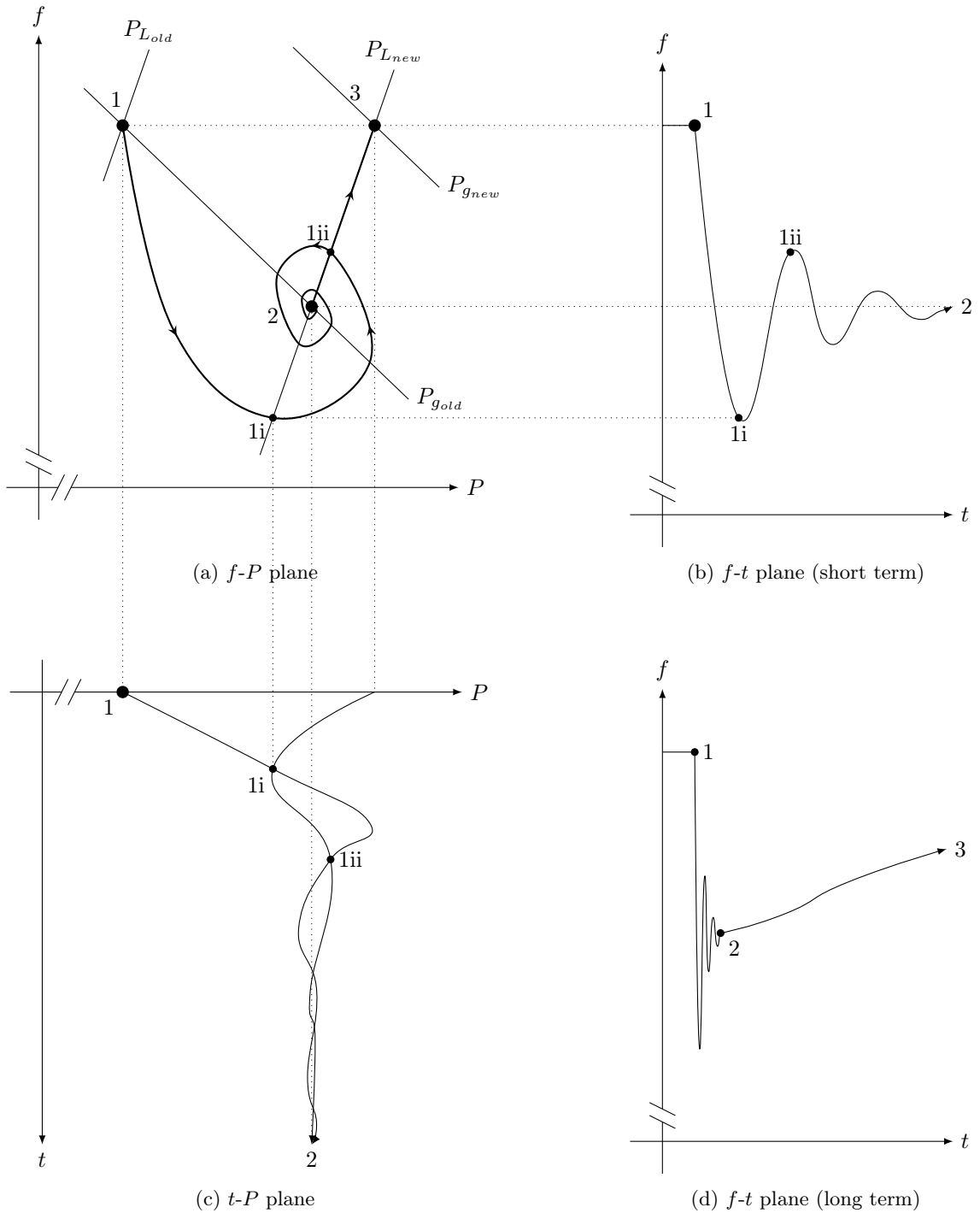


Figure 5: Transient behaviour for step increase in demand. (a) The power-frequency operating point moves from 1 to 2 due to droop and load relief, via 1i and 1ii. Secondary action shifts the generation curve from $P_{g_{old}}$ to $P_{g_{new}}$, bringing the operation to point 3. (b,d) Corresponding frequency drop over time after the step increase in load. (c) Load and generator power output oscillations over time during the transient. Generation is the curve which starts at point 1.

will decrease. This poses operational challenges because the ROCOF during frequency excursions will be higher [5].

Many grid operators currently require that distributed generation disconnect from the grid during under frequency events. Such disconnections would reduce the amount of generation available during an under frequency event, which would exacerbate the frequency excursion, and may even lead to network instability. Reduced inertia causes increased transient currents over inter-region ties. This can trip protection systems in already critical moments [4].

In a high renewables grid, inertia will be lowest during the middle of the night [11]. This is because total demand at night is low, so relatively expensive conventional generators will get switched off, leaving mostly cheap inertia-less renewables to supply power.

Some network operators are so concerned about the operational challenges associated with the lack of inertia due to increased renewables that they enforce strict upper limits on renewable penetration levels. Ireland and the French Islands have operational caps of 50% and 30% respectively [11, 15]. In contrast a study conducted by General Electric for the Californian electricity network operator concluded that the displacement of inertia due to 50% renewables penetration is manageable (in California's grid), through an increase in governor action, demand response and other similar mechanisms [16]. In particular they recommended the injection of power from energy storage devices for frequency regulation, which is discussed in the following section.

II.1.6 Proposed Solution

Power electronics can be extremely fast and flexible compared to conventional loads and generators [13]. There is much literature concerning the addition of frequency sensitive control loops to the power electronics interfaces of modern generators so that they can support frequency regulation [2, 4, 6, 8, 11, 17, 18, 19, 20]. Such functionality is called *synthetic inertia*, *virtual inertia* or *inertia emulation*. In a high renewables, low inertia grid, inertia emulation in aggregate could hopefully replace and possibly exceed the conventional inertia which has been displaced.

II.1.6.1 Variable Speed Wind Turbines

The most well developed form of inertia emulation is that of variable speed wind turbines [17]. As mentioned in Section II.1.1, modern variable wind speed turbines normally do not contribute inertial response to the grid, despite the plant possessing rotational inertia. This is because the tip speed is decoupled from the grid frequency by the power electronics interface. By adding a frequency sensitive control loop to the power electronics interface the kinetic energy of the spinning blades can be harnessed.

During under frequency events the controller extracts kinetic energy from the spinning blades, thereby slowing them down so that extra energy can be injected into the grid to oppose the frequency drop. Since the rotational frequency of the turbine is still decoupled from the network, the blades can be slowed down by more than the drop in electrical frequency. This allows such variable speed wind turbines to be more effective at arresting frequency drops than both fixed speed turbines and conventional generators (when comparing initial additional energy injection relative to nameplate capacity) [8, 11]. Several wind farms already have inertia emulation functionality, indeed several utilities worldwide already mandate that large wind farms must emulate inertia [8].

II.1.6.2 Storage

Batteries, fuel cells and super-capacitors have no moving parts, so they do not have any inherent inertia. However they are extremely flexible and fast, so they can be controlled to emulate the inertial behaviour (and droop characteristics) of conventional generators [4, 6, 18]. Inverters with such control are called virtual synchronous machines (VSMs) [19]. Inverters are so fast and flexible that they can even provide greater support per unit of nameplate capacity than conventional generators [13, 16].

Unlike wind turbines, storage devices offer bidirectional flexibility. They can increase their charge rate or decrease their discharge rate to help bring the network frequency down. They can also decrease their charge rate or increase their discharge rate to push the network frequency up.

Since frequency deviations are generally short lived, the ratings on some inverters and storage devices may be temporarily exceeded, to provide the maximum possible support to the grid [20]. This reduces the lifespan of the device. Even without exceeding the ratings, inertia emulation functionality still places extra strain on the inverter and storage, thereby reducing its lifespan [2].

Under-frequency and over frequency support are needed in different quantities. In general the two do not cancel out. Therefore any storage device offering frequency support will tend towards full charge or full discharge, at which point they can no longer offer support for one direction of frequency deviation. This poses a challenge for VSM controllers. Aghamohammadi and Abdolahinia proposed an inertia emulation algorithm which accounts for the state of charge of a battery [20]. Borsche et al. proposed a similar algorithm which also utilises a deadband in the controller to solve this issue [21].

In addition to solving state of charge issues, adding deadband to the VSM controller offers other benefits. The inherent delay of the inertial response of VSMs might pose stability issues in a grid with many VSMs. Deadband may address this [16]. Nanou et al. used a 500 mHz deadband in the controller in their simulations, to match the specifications of their local utility [18]. Serban and Marinescu used a 20 mHz deadband to avoid the controller integrating a frequency measurement error, and to more closely replicate classical mechanical regulators [22].

Torres and Lopes simulated a VSM in a microgrid [19]. The chosen controller was a proportional and integral (PI) controller in the synchronous reference frame. One advantages of controlling in the synchronous reference frame is that reactive power and real power can be easily controlled independently. Furthermore PI controllers have no steady state error in the synchronous reference frame, but they do in the natural reference frame. Torres and Lopes chose parameters to emulate the characteristics of one of the diesel generators in their microgrid. Frequency variations for two diesel generators and a wind turbine were compared with one diesel generator, a wind turbine and a VSM. Their simulation results showed that the VSM performed better than the diesel generator. That is, the frequency deviations were slower and smaller when the diesel generator was replaced with a VSM of equal nameplate capacity.

Torres and Lopes chose control parameters so that the performance of their VSM matched a conventional generator. In contrast Serban and Marinescu used trial and error to choose parameters which resulted in the best frequency performance [22]. Torres et al. later proposed a dynamic algorithm which chooses control parameters using an exhaustive search, and these parameters change over time [23]. This algorithm was very computationally expensive, and there was little improvement in frequency performance. However there was a far higher efficiency compared to static parameters. That is, the storage device consumed less energy through losses, per unit of reduction in frequency deviation. Delille

et al. also proposed a wait time of 10 minutes before recharging after a significant event, to avoid higher than normal power draw during a sensitive period [24].

Inertia emulation has been trialed through the deployment of a super-capacitor in Hawaii in 2006 [24]. It successfully helped stabilise the grid, however it was destroyed by an earthquake after only a year of service. The aforementioned studies which discussed batteries only involved simulations. This literature review shows that inertia emulation has not been experimentally trialled using batteries [24].

II.1.6.3 Commercial Incentives

Inertia emulation provides a valuable service to the network. However as discussed above, it can place extra strain on the plant, and involves an upfront cost during design and manufacture of the control system. There should be financial incentives in place which are sufficient to overcome these costs to encourage manufacturers and generator operators to implement inertia emulation. There are currently minimal such incentives. Both General Electric and Muljadi et al. suggest that there should eventually be *inertia markets* to provide such incentives [16, 17].

The FCAS markets in the NEM do not include inertia markets. The rules allow participating in the FCAS markets with an aggregation of distributed generation and load for arresting large frequency excursions, but they currently prohibit it for normal frequency regulation [12]. Re却it Power is a market player who aggregates the PV and storage of their customers and bids into the electricity markets on their behalf. They currently use local frequency sensing to rapidly change consumption and generation rates during frequency excursions [25]. In this way they are already providing a viable form of frequency support from inertia-less plant. Despite the lack of dedicated financial incentives, this work is probably commercially viable today.² This functionality is relatively rudimentary compared to the VSMs, due to the current lack of financial incentives for more sophisticated approaches.

II.2 Inverters

II.2.1 Switching

The structure of a typical two level, three phase inverter is shown in Figure 6. By turning on one switch per branch at a time, and alternating between them extremely frequently with a given duty cycle, the average output can be any arbitrary voltage within the DC supply range. To generate three balanced sinusoidal voltages at the output, each leg is controlled with a pulse width modulation (PWM) sinusoid. Freewheeling diodes are also present across each transistor to avoid open-circuiting the output terminals.

When simulating inverters the PWM signal generation and the switching itself can be approximated as three controlled voltage sources [26], if the switching frequency is high enough. This approximation simplifies the computations greatly, which leads to faster simulations with negligible loss of accuracy.

²Due to the commercially sensitive nature of their work, some details are not publicly available.

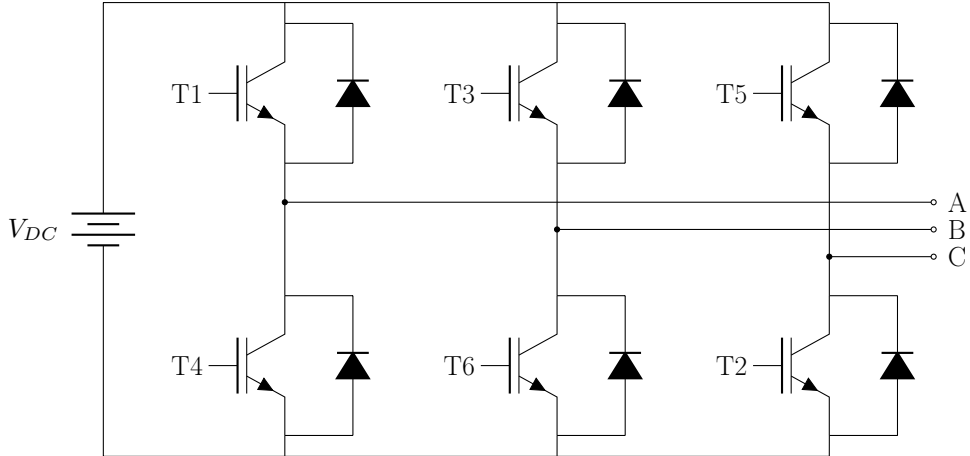


Figure 6: Typical three phase, two level inverter, excluding filtering.

II.2.2 Filtering

The output of the switching process has high frequency components at the carrier frequency. This is undesirable for connection to the grid or most loads. Since the switching frequency is several orders of magnitude higher than mains frequency, these high frequency components can be easily filtered out. The two most common types of filter are LC and LCL, which are shown in Figure 7.

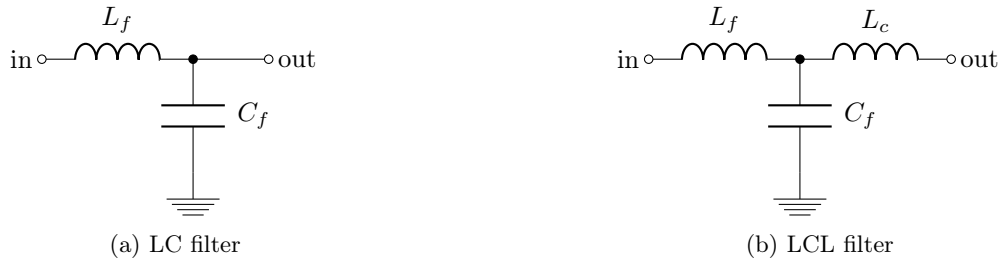


Figure 7: Common inverter output filters

II.2.3 Control

There are four main control architectures for inverters [2].

Grid forming inverters act as a voltage source. This architecture is typically used for stand alone operation. Grid forming inverters do not work well when in parallel with other grid feeding sources.

Grid feeding inverters act as a current source. They inject a current corresponding to a pre-existing network voltage. As such, a grid cannot operate with solely grid feeding inverters. There must be a different type of inverter, or a conventional generator on the network.

Grid forming and grid feeding inverters can be modified with the addition of *droop* so that loads are shared between multiple generators more equally, and they help contribute to frequency and voltage regulation. These are called *grid supporting grid forming* and *grid supporting grid feeding* inverters respectively. This thesis mainly deals with *grid supporting grid feeding* inverters.

Part III

Problem Statement

III.1 Context

The literature review has shown that there has been much investigation into battery based VSMs using simulations, however there have been no attempts to construct such a device and test it experimentally.

Inertia emulation can be implemented in batteries, fuel cells, wind turbines and more. Batteries have been chosen as the focus of this thesis because

- the penetration levels of batteries are expected to increase greatly over the coming decades;
- inertia emulation with wind turbines has been thoroughly investigated, whereas there is much more to be learnt for batteries;
- unlike wind, PV and other generation sources, batteries can both sink and source power; and
- unlike wind, PV and other power constrained generation sources, batteries are often operated at less than 100% capacity because they are energy constrained, rather than power constrained.

III.2 Goal

The goal of this thesis was to construct and test the first ever battery based VSM by adding droop control and inertia emulation to an inverter, to experimentally prove or disprove that such a system can successfully mimic the inertial behaviour of conventional generators.

Part IV

Design

IV.1 Constraints

The inverter used in the experimental setup runs C code on a TMS320F2810 digital signal processor (DSP), which has no floating point unit. The existing control system uses a 20 kHz interrupt. There is only $30\ \mu s$ of idle time between interrupts, within which the code for droop and inertia emulation must be completed. Therefore the core control code must be extremely efficient. Only fixed point arithmetic was used in the core control interrupt, with the number of fractional bits varied throughout the code to maximise accuracy.

The control system code is loaded into random access memory (RAM) instead of flash memory, to increase the speed of execution. Consequently there is a small code size limit.

The inverter was designed and manufactured by Creative Power, who made the code for the control loop available, and added several empty functions which hook into the state machine, through which custom functionality can be added. However many parts of the code remain inaccessible. The core current control loop is implemented with 16 bit variables, with a scaling factor that results in utilisation of less than the full scale. Consequently the resolution of the current control loop is approximately 0.5% of full rated current, due to rounding errors. This is not ideal, but cannot be rectified because the relevant code is not fully accessible.

The inverter protection systems trip at a ROCOF of approximately 0.13 Hz/s. This relatively low threshold cannot be increased, because the relevant code is not accessible.

Different models of inverters may not have the same constraints. This particular model was chosen because it was readily available, and because it is designed to safely run experimental code.

IV.2 Control Architecture

The existing control system uses an inner proportional-resonant (PR) current control loop, surrounded by an optional outer PI DC voltage regulation loop. When the inverter is connected to a battery, the battery system would regulate the DC voltage. The experimental setup described in Part VI uses a laboratory DC power supply instead of a battery, which also ensures that the DC bus is externally regulated. Consequently the outer voltage regulation control loop is not necessary in this context. A graphical Simulink model of the existing control system is shown in Figure 9 on page 18, in current controlled mode, without the voltage regulation loop.

The voltage regulation loop was replaced with a power control loop, which takes the grid frequency as an input and outputs the setpoint for the inner current control loop. This is shown in Figure 10 on page 19. Since a single inverter cannot impact the grid frequency significantly, a compensator would saturate whenever the grid voltage is not precisely the nominal voltage. Assuming the grid voltage does not change quickly, the output current is proportional to the output power. Consequently the power control loop simply determines the desired output power based on frequency (for a given amount of droop and inertia) and calculates the corresponding current setpoint. However in order

to maximise computational efficiency, the power control loop does not divide desired power by the AC voltage to obtain the desired current. Instead such division occurs at compilation time and in a less frequent background task, thereby keeping all calculations in the same scale as current. Since the background tasks occur less frequently, there is sufficient time to conduct floating point divisions and other computationally expensive tasks. The assumption that grid voltage is approximately constant only needs to be true over the interrupt period of this less frequent background task.

The contributions of droop and inertia emulation to power output are calculated separately, and then superimposed on the power setpoint. The resulting power target is passed through a saturation block, to prevent the target current from exceeding the inverter's ratings. This is shown graphically in Figure 8, where Id and Iq refer to the direct (real) and quadrature (reactive) components of current respectively.

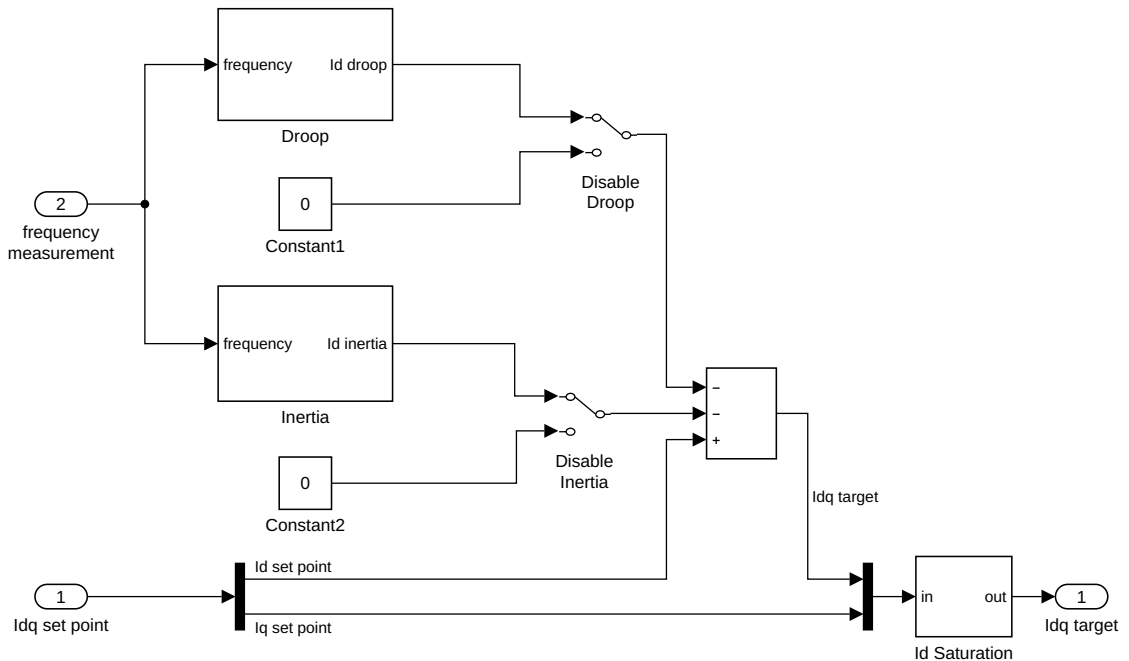


Figure 8: Current control calculation architecture. Droop and inertia contributions are calculated in parallel and subtracted from the nominal real current setpoint. The reactive current setpoint remains unchanged.

IV.3 Droop

Power-frequency ($P - f$) droop functionality was added to the inverter control system. That is, code was written to implement the curve shown in Figure 3 on page 7.

Voltage ($Q - V$) droop is typically used to control network voltage. There is no reason why VSMs cannot also provide voltage regulation in addition to frequency regulation. However the scope of this thesis has been limited frequency regulation, and not voltage regulation. Consequently voltage droop was not implemented.

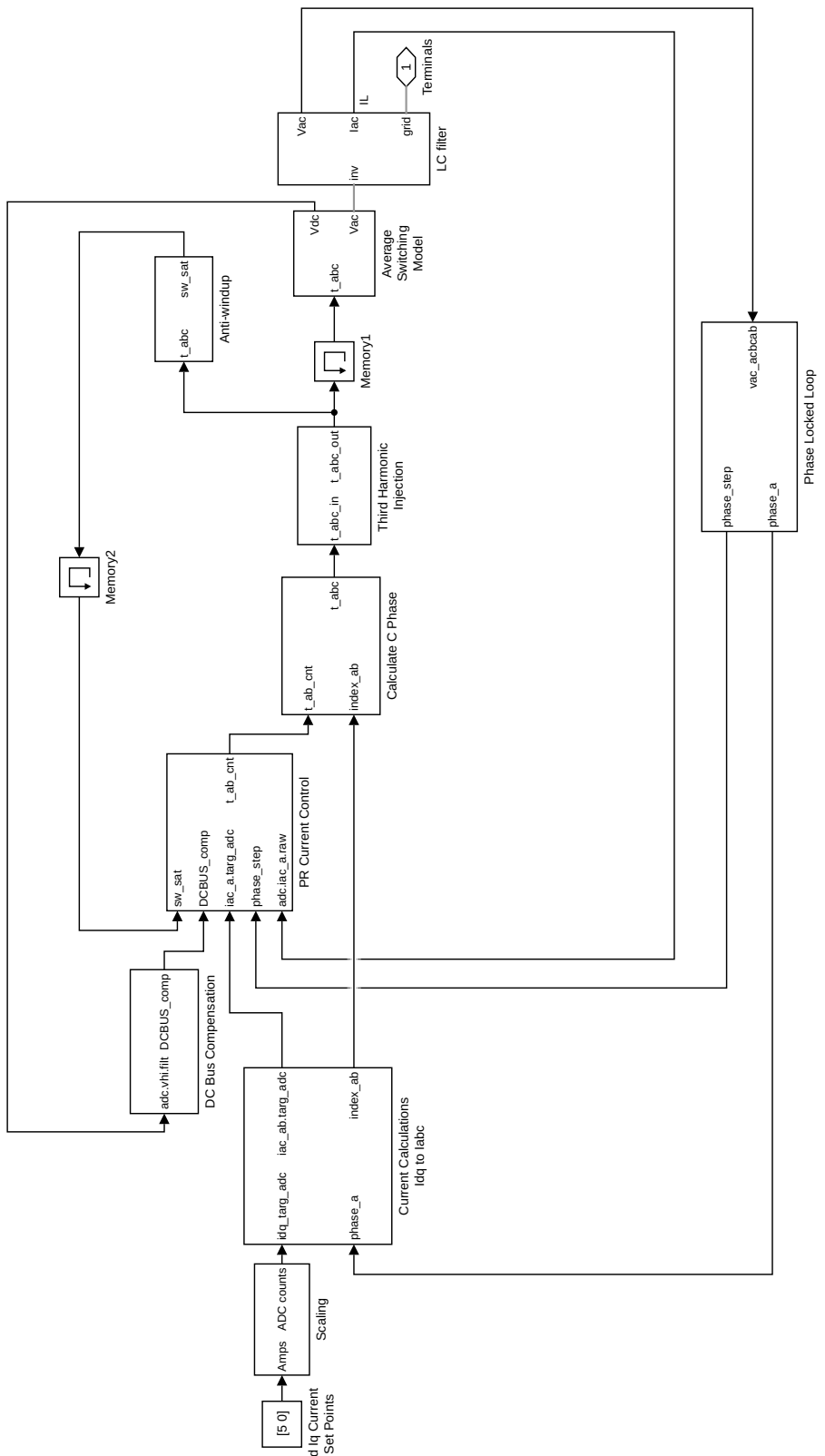


Figure 9: The pre-existing inverter control system, which uses a PR current control loop in the natural reference frame.

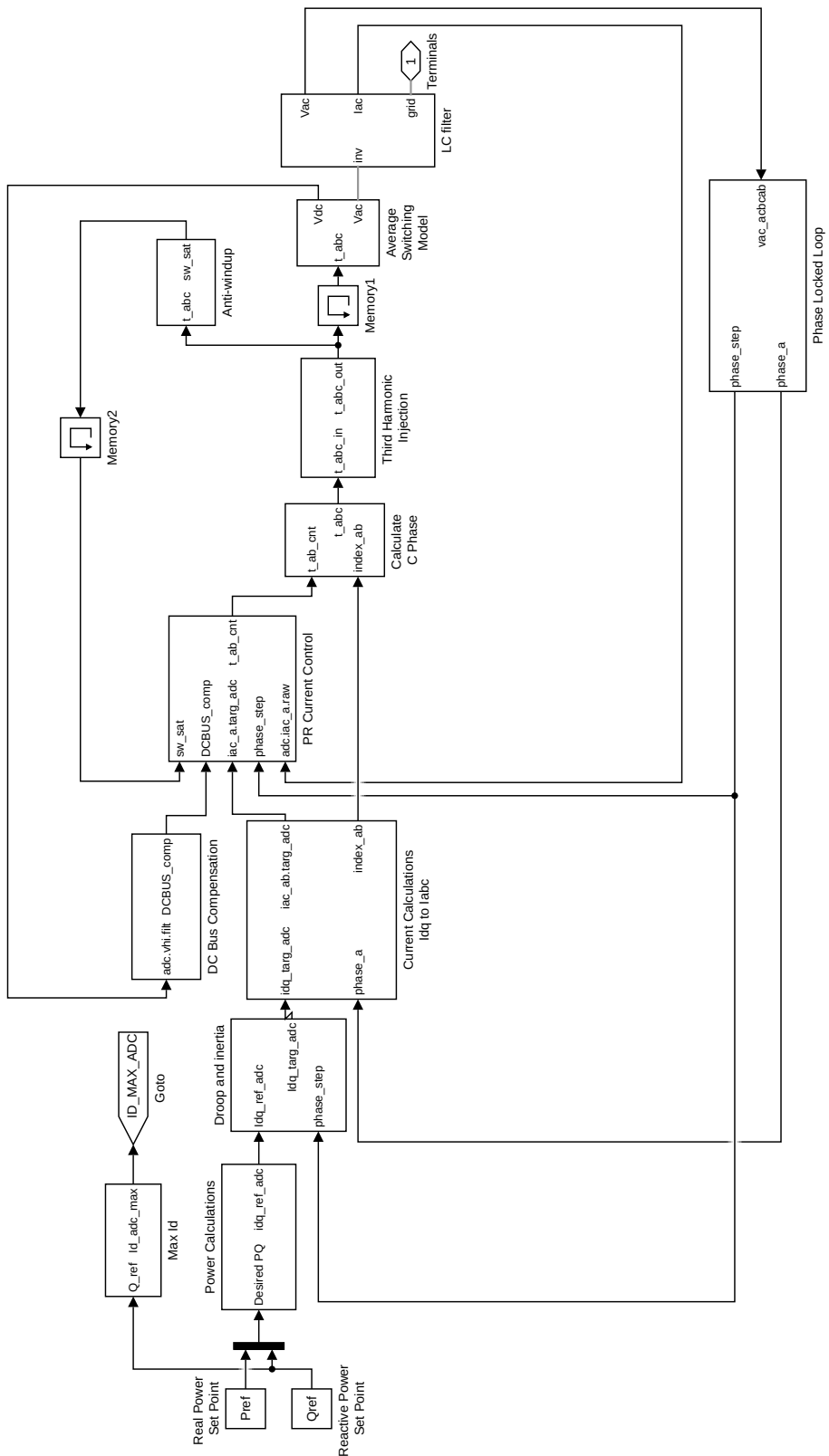


Figure 10: Inverter control system with inertia and droop added in an outer power control loop, which wraps around the pre-existing current control loop.

In floating point, the droop arithmetic is given by

$$\Delta P = -\frac{\Delta f}{f_{nom}} \times \frac{P_{max}}{K_{droop}} \quad (7)$$

Where

- ΔP is the component of output power due to droop;
- $\Delta f = f - f_{nom}$ is the deviation of grid frequency from nominal;
- P_{max} is the power rating of the inverter;
- f_{nom} is the nominal frequency (50 Hz); and
- K_{droop} is the amount of droop (4%), which means that a 4% change in frequency causes a change 100% change in output power, which is P_{max} .

As mentioned in Section IV.2, the code calculates everything in the same scale as current. So Equation 7 is implemented as Equation 8.

$$\Delta I_d = -\frac{\Delta f \times I_{max}}{(f_{nom} \times K_{droop})} \quad (8)$$

Where

- I_d is the direct component of current in the rotating reference frame, which is proportional to real power;
- ΔI_d is the component of I_d due to droop; and
- I_{max} is the rated current.

The reciprocal of the denominator is calculated at compilation time, so only one fixed point multiplication takes place at runtime to evaluate Equation 8.

The error in frequency measurement by the PLL was found to be up to 0.04 Hz. Consequently a deadband of ± 0.05 Hz was added to the frequency measurement (Δf).

IV.4 Inertia

Inertia emulation involves adjusting the desired real output power based on the time derivative of the network frequency. Taking the time derivative of Equation 1 on page 5 and substituting in Equation 4 on page 6 yields Equation 9.

$$P_{inertia} \approx \frac{2HS_n}{f_{nom}} \times \frac{df}{dt} \quad (9)$$

Where

- $P_{inertia}$ is the inertial component of real output power;
- H is the inertia constant;
- S_n is the nameplate power rating (5 kVA);
- f_{nom} is the nominal frequency (50 Hz); and
- $\frac{df}{dt}$ is the time derivative of frequency.

For a discrete control system with interrupt frequency f_{int} , this becomes

$$P_{inertia} \approx \frac{2HS_n}{f_{nom}} \times \Delta f \times f_{int} \quad (10)$$

Rephrasing Equation 10 to be in the same units as current (as explained in Section IV.2) gives

$$I_{d_{inertia}} = \frac{2HI_{max}}{f_{nom}} \times \Delta f \times f_{int} \quad (11)$$

This inertia emulation algorithm contains no deadband, because the need for it did not arise during experimental testing.

After the peak of a frequency deviation once frequency starts returning to nominal, conventional inertia acts to oppose the change of frequency, thereby hindering the return of grid frequency to the nominal value. Grid operators wish to hasten the return of grid frequency to nominal after an excursion. Therefore this behaviour is undesirable. With inertia emulation, the inertial response can be disabled on the return swing towards nominal, thereby hastening frequency restoration. Such novel functionality is an original contribution of this thesis. It will be referred to as *directional inertia*. Directional inertia was implemented and tested for this thesis. The code uses relatively simple IF statements, to implement the logic shown in Table 1. Directional inertia should hasten the return of frequency to nominal, which is desirable. However there are downsides to such behaviour, which are discussed in Section VIII.5 on page 48.

Table 1: Logic for inertia contribution with directional inertia.

	Frequency Increasing	Frequency Decreasing
Over Frequency Event	Enable	Disable
Under Frequency Event	Disable	Enable

Ideas similar to directional inertia have been proposed by Torres et al. and Delille et al. [23, 24]. Torres et al. proposed disabling inertia emulation during the latter oscillations of a frequency deviation, for the purpose of reducing the instability risk posed by VSMs with a non-negligible response time. Torres et al. made no attempt to investigate such an idea. Delille et al. investigated an algorithm where frequency support is gradually disabled 10 s after a frequency event, once primary control has fully actuated. The support in question was not the same as inertia emulation, and is more similar to the work done by Reposit Power, which is discussed in Section II.1.6.3 on page 13. Both of these ideas are similar yet distinct from the directional inertia proposed above.

IV.5 Frequency Measurement

A phase locked loop (PLL) is a system which measures frequency. The PLL used for inertia emulation must adhere to stringent requirements. Real inertia responds instantaneously to frequency deviations. Therefore an ideal VSM should detect frequency changes and ROCOF changes as quickly as possible, whilst rejecting noise. An underdamped PLL will respond to a step change in frequency with overshoot and subsequent ringing. The derivative of such a signal will oscillate wildly, which is very undesirable. The PLL must also measure frequency and its derivative with great steady state accuracy. The existing PLL used in the inverter for this experiment did not meet many of these requirements. The accuracy was poor due to rounding errors, and the rise time in response to a step in frequency was slow. Consequently a new PLL was implemented, using the design described by Phipps et al. [1]. This design was chosen because unlike most PLL designs, it lacks a Clarke transform, and is consequently far more computationally efficient. A Simulink model of the PLL is shown in Figure 11.

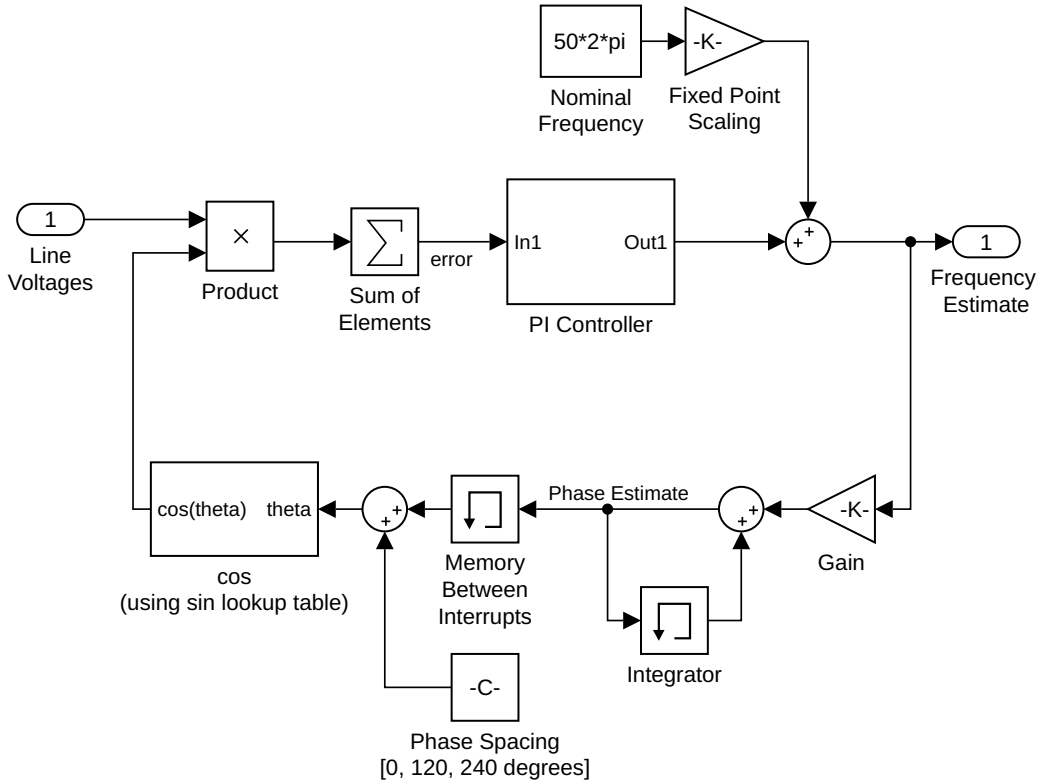


Figure 11: PLL Design. An estimate of phase is obtained from the frequency estimate. The error between phase estimate and measured voltage is calculated in the natural reference frame. The error is passed through a PI controller and added to nominal frequency to obtain the new frequency estimate.

The constants for the PI controller in the PLL were initially chosen using Matlab's PI controller design tool. The constants were then tweaked by hand during simulation and experimental testing, in order to co-optimise the system with the subsequent filter. The PLL was empirically found to be as fast as possible (whilst still stable) with proportionality and integral constants equal to 5 and 20 respectively. However a proportionality constant of 0.01 was chosen instead, despite the reduction in PLL speed. This was because the output of the PLL was far less noisy with a smaller proportionality constant, which resulted in less filtering being necessary. Since the propagation delay and rise time of the filter

are far longer than for the PLL, this co-optimisation resulted in a net decrease in the overall system's response time by a factor of 6.

Since the PLL has 3 AC inputs and one DC output, and is implemented in fixed point, it is difficult to prove its stability algebraically. Instead the PLL was tested through simulation and experiment with a step change in frequency. The rise time of the step corresponded to a slope of 0.7 Hz/s, which is far higher than the protection threshold of 0.13 Hz/s mentioned in Section IV.1.

The PLL was implemented in fixed point, for computational efficiency. The phase estimate (obtained by integrating the frequency estimate) was deliberately scaled so that overflow occurs at a phase of 2π radians. Consequently there need not be any checks for overflow, nor modulo operations to wrap the phase. The cosine operation is computed using the pre-existing sine lookup table. The number of fractional bits varies throughout the PLL loop, in order to maximise accuracy, by setting the dynamic range to approximately 0.7 Hz/s. The number of fractional bits was also chosen to co-optimize the accuracy and dynamic range with the subsequent filtering and derivative.

IV.6 Filtering

IV.6.1 Motivation and General Requirements

Inertia emulation involves taking the derivative of frequency, which necessarily exacerbates high frequency components in the estimate of frequency. Consequently the measurement of frequency and its derivative must be passed through a low pass filter. However if the filtering is too heavy, then the response time will be compromised. This delicate balance is discussed further in Section VIII.4 on page 47.

An advantage of using finite impulse response (FIR) filters over infinite impulse response (IIR) is that it is easier to guarantee stability for FIR filters. Furthermore, the maximum dynamic range of any signal in a FIR filter is trivial to calculate, which makes fixed point design relatively straightforward. However since the desired cut off frequencies are 3 orders of magnitude lower than the sampling frequency, an FIR filter would require hundreds or thousands of coefficients and delays. There are stringent speed and memory requirements, so this is not acceptable. One solution would be to significantly decimate the input signal, however this would reduce the performance of the filter. Consequently IIR filters were chosen over FIR filters.

IV.6.2 Frequency Filter

The filter was designed using Matlab's filter design tool, with the following requirements:

- Passband frequency of 1 Hz
- Stopband frequency of 10 Hz
- Stopband attenuation of 50 dB

The passband and stopband frequencies were chosen to be a whole decade apart, to minimise the complexity of the filter. A stopband frequency of 10 Hz was chosen based on the overall system speed requirements discussed in Section VIII.4.3 on page 48. The resulting filter is fourth order, split into 2 stages, which is shown in Figure 12.

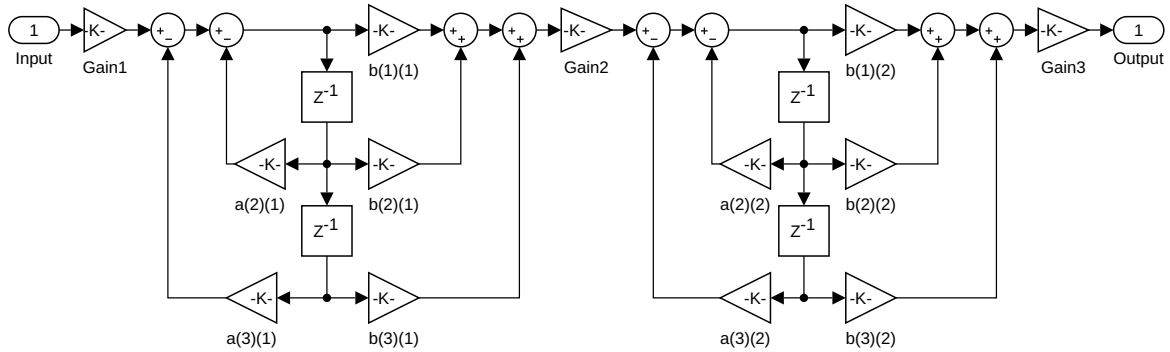


Figure 12: IIR Filter Structure, using two cascaded second order stages in direct form II.

The operation of IIR filters tends to result in very large signals in the feedback loop. Consequently the number of fractional bits used for the feedback gains cannot be too high, because that would result in saturation, which leads to overflow that corrupts the output. However if the number of fractional bits used for the feedback gains is too small, then rounding errors will alter the coefficients values, and hence the filter's performance. It was found that even a 0.5% rounding error in the feedback loop results in instability in the feedback loops.

The difference between too many fractional bits and too few was empirically tested through trial and error in Simulink. It was discovered that the acceptable number of fractional bits differs between each constant. Furthermore the range of bits which does not result in saturation or unacceptable rounding errors is very small, typically 1 or 2 bits. For example, the first feedback gain uses 22 fractional bits. If 23 fractional bits are used, saturation occurs³. If 21 fractional bits are used, the rounding error results in instability.

This extremely narrow range of acceptable fractional bits posed a challenge during the design process. Consequently the filter was implemented using 64 bit integers, whereas most of the existing control system is implemented with 16 bit integers. In order to determine the acceptable number of fractional bits for each coefficient, the range of values at the output of the respective coefficient in a floating point simulation was observed (since this cannot be easily calculated by hand, due to the complexity of the double feedback), and the number of fractional bits was set so that this corresponds to the largest integer possible which is less than 2^{64-1} .

IV.6.3 Frequency Derivative Mean

A crude yet computationally cheap rolling mean was added after the discrete derivative, to reduce the high frequency noise. Summing all samples in the window each interrupt would be very costly. Instead the sum is saved between interrupts, and is incremented by the value of the new sample, and decremented by the value of the sample which is leaving the window. This is far faster to compute.

The window size of the rolling mean was chosen deliberately to be a power of 2, so that the division of the sum of the samples by the number of samples can be implemented using a cheap bit shift, rather

³For a noisy sinusoidal input signal with a maximum slope equal to the maximum slope the PLL is designed for, and frequency equal to the filter stopband frequency.

than an expensive division. Furthermore, when the index into the circular array is incremented, it can be wrapped using a cheap bitwise AND operation, rather than a more expensive modulo operation. The window size of the rolling mean was chosen to be 2^5 , since that was empirically found to be the lowest size which results in acceptable performance.

IV.7 Power Setpoint Saturation

For large and fast frequency deviations the droop and inertia components of the desired output can exceed the ratings of the inverter. Consequently the desired power output must be saturated prior to the current control loop. There are two possible approaches to saturating desired power when it exceeds the ratings.

1. Scale down both real and reactive power by the same percentage; or
2. Keep reactive power the same, and scale down only real power.

Droop and inertia only change the real power, and not the reactive power. The 5 kVA rating for the inverter is for apparent power. Option 1 results in a decrease of reactive power during frequency disturbances, which is not desirable. Option 2 was chosen, since saturation will only occur due to changes to the desired real power.

To implement option 2, the real power must be saturated at

$$I_{d_{max}} = \frac{\sqrt{S_{max}^2 - Q^2}}{3V_{ac}} \quad (12)$$

Where

- $I_{d_{max}}$ is the maximum direct current in the rotating reference frame, which is proportional to real power;
- S_{max} is the power rating of the inverter;
- Q is the reactive power setpoint; and
- V_{ac} is the root mean squared (RMS) phase voltage of the grid.

Equation 12 is computationally expensive, since it involves a square root calculation, as well as a division by a variable. To allow the core control interrupt to be completed within the stringent time requirements, $I_{d_{max}}$ is computed and saved each time the reactive power setpoint (Q) is changed. This shifts the computational burden from the time critical interrupt to the initialisation and user interface code, where even a 1000 ms execution time is acceptable.

The inverter used has both power and current ratings, which differ when the grid voltage is not nominal. The saturation code considers both, and saturates to the minimum of the current and power limits. Experimental results demonstrating the correct operation of this saturation functionality are included in Appendix B on page 56.

Since the DC supply used in the experimental setup cannot sink current, the lower saturation limit was set to 0 W, not $-I_{d_{max}}$.

Part V

Simulations

V.1 Motivation

The specific inverter used in the experimental setup was modelled in Simulink, to aid the development of the code and parameters used in the experimental tests. The model matches the components and structure of the inverter, as well as the exact C code used for the pre-existing control system. Incorporating the exact C code was crucial for ensuring that the fixed point arithmetic in the new code was correct, prior to commencing physical tests, as well improving the accuracy and speed of the simulations.

Simulink was chosen over other simulation software because

- it is relatively easy and seamless to simulate hybrid continuous and discrete models;
- the results can be easily and immediately processed using *Matlab*'s base functionality; and
- it is possible to include the exact C code used in the inverter, alongside native simulation blocks.

V.2 Switching Model

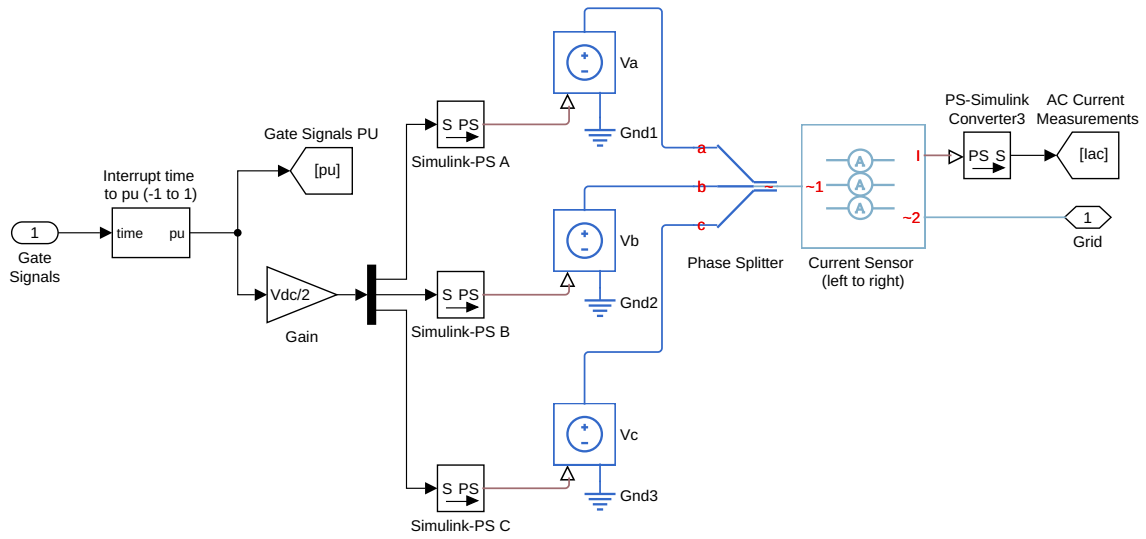
The inverter model utilises the average voltage source model described by Paquette [2] and Shepherd [27], which is shown in Figure 13a. This model abstracts away the PWM signal generation and switching. This results in simulation times which were found to be faster by 3 orders of magnitude. However this average model has several limitations.

Consider the example edge case of an input control signal of 300 V (instantaneous) for all three phases. Such an unbalanced signal would not occur during normal operation. However consideration of such edge cases helps verify correct modelling. In Shepherd's average voltage source model all three outputs will be pulled to 300 V. Due to the floating DC supply in a practical inverter (shown in Figure 6 on page 14), such an input signal should result in all three phase legs being shorted together and floated relative to ground, even if the DC supply is larger than 300 V. Similarly, with Shepherd's model third harmonic injection would result in all three phase voltages being increased by the same amount, which does not match the behaviour of third harmonic injection in practical inverters. Therefore the average voltage source model as described by Shepherd has shortcomings.

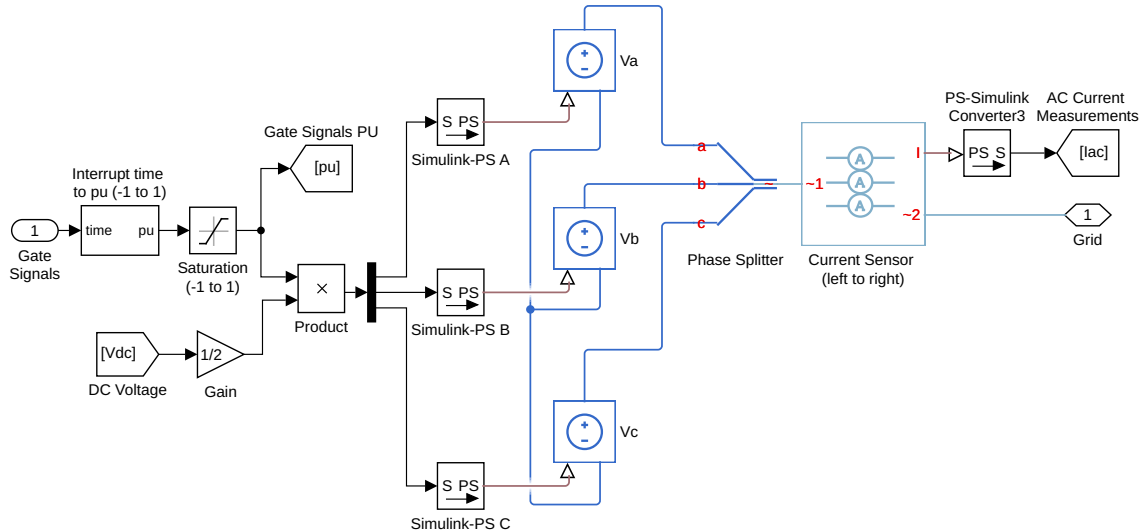
The first improvement made to the model in this thesis is that the star point is now floating, which addresses this issue. This change can be seen in Figure 13.

Paquette's model does not attempt to include saturation. The model can output arbitrarily large voltages, when in reality the battery or PV array supplying an inverter has a finite voltage, and the modulation index ranges between 0 and 1. Saturation was added to the input signals to clip the phase voltages between 0 V and the DC voltage.

Modelling saturation accurately is important because saturation and current ratings are the factors which limit the amount of inertial support that an inverter can provide.



(a) Model from the literature [2]



(b) Improved model

Figure 13: Improvements to average voltage source approximation for three phase inverter to account for switching saturation. The star point is now floating, the simulated DC bus voltage is used, and the input signal is saturated.

To simulate the DC side of the average switching model, a controlled current source was used, with an input equal to the sum of the average currents. For a modulation index of 0.5, the average current is 0 A, because the current is drawn from the positive DC bus 50% of the time, and from the negative 50% of the time. For a modulation index of 1, the branch is shorted to the positive DC bus, so the current drawn from the DC side equals the average current drawn by the grid. For a modulation index of 0, the branch is shorted to the negative DC bus, so the average current drawn from the DC side equals the negative of the average current drawn by the grid. Therefore the current in the DC side for each phase equals the product of the current in the AC side, and the gate signal (when scaled from -1 to 1). This is shown in Figure 14. Transport delays of negligible time were added to allow the simulation solver to converge.

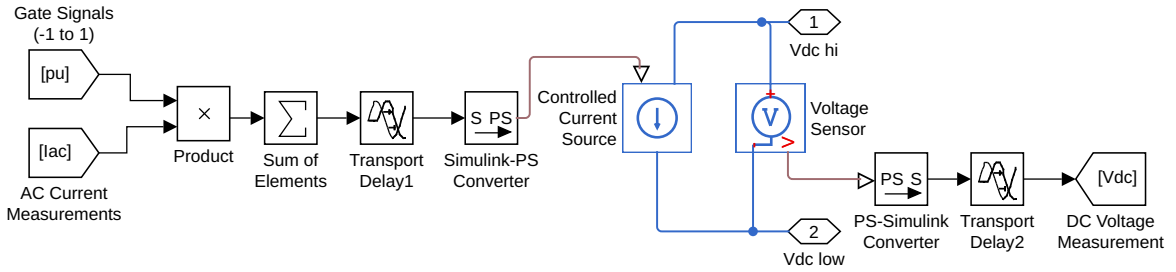


Figure 14: Average switching model for the DC side. Each instantaneous phase leg current is scaled by the gate signal (from -1 to 1), and summed together to produce the average DC current.

To simulate soft charging of the DC bus capacitors from the AC side a set of 6 diodes was placed in parallel with the average switching model, matching the configuration of the insulated gate bipolar transistor (IGBT) protection diodes through which soft charging occurs.

The resulting switching model is able to quickly simulate both the DC and AC side of the switches, including soft charge transients at startup.

V.3 Limitations

The model developed for this thesis includes the exact C code used for the steady state control of the specific inverter used in the experimental setup. Some of the remaining code was not made available by the manufacturer. Consequently some unrelated aspects of the inverter's operation such as fault detection and phase sequencing could not be simulated.

V.4 Verification of Experimental Approach

The experimental method described in Section VI.1 does not measure the impact of inertia emulation on grid frequency. Rather, it tests how closely the output power of a VSM matches that of a synchronous machine, and assumes that the impact on grid frequency would be the same as that of a synchronous machine with the same amount of inertia. Simulations were conducted to verify this assumption.

Simulating thousands of inverters in a full sized grid with the full detail of the control system is beyond the scope of this thesis. Instead a microgrid was simulated, with a single synchronous generator, and an

inverter. The synchronous generator has a 14 kVA rating, and an inertia constant of 4 s. The inverter model matches that of the inverter used in the experimental setup, including hardware, control system and settings. A step increase in load from 5 kW + 0.75 kVAR to 6.7 kW + 0.75 kVAR was simulated, and frequency drops as expected.

The output power of the inverter and the grid frequency are shown in Figure 15. As expected, the frequency deviation is smaller when the inverter has droop control. With inertia emulation too it is slower and even smaller.

These simulation results show that inertia emulation does reduce the speed and magnitude of frequency deviations, in at least the microgrid which was simulated. Future work on this topic should include simulations of a full sized grid. A more comprehensive full grid simulation would account for the interaction between multiple inverters and synchronous machines, network impedances, voltage sags and swells, and other complexities of scale.

Since the experimental results confirm that the design works and matches simulations, these simulation results support that claim that VSMs will reduce the speed and magnitude of frequency deviations. That is, the assumption mentioned above is a valid assumption, so the experimental approach is sound.

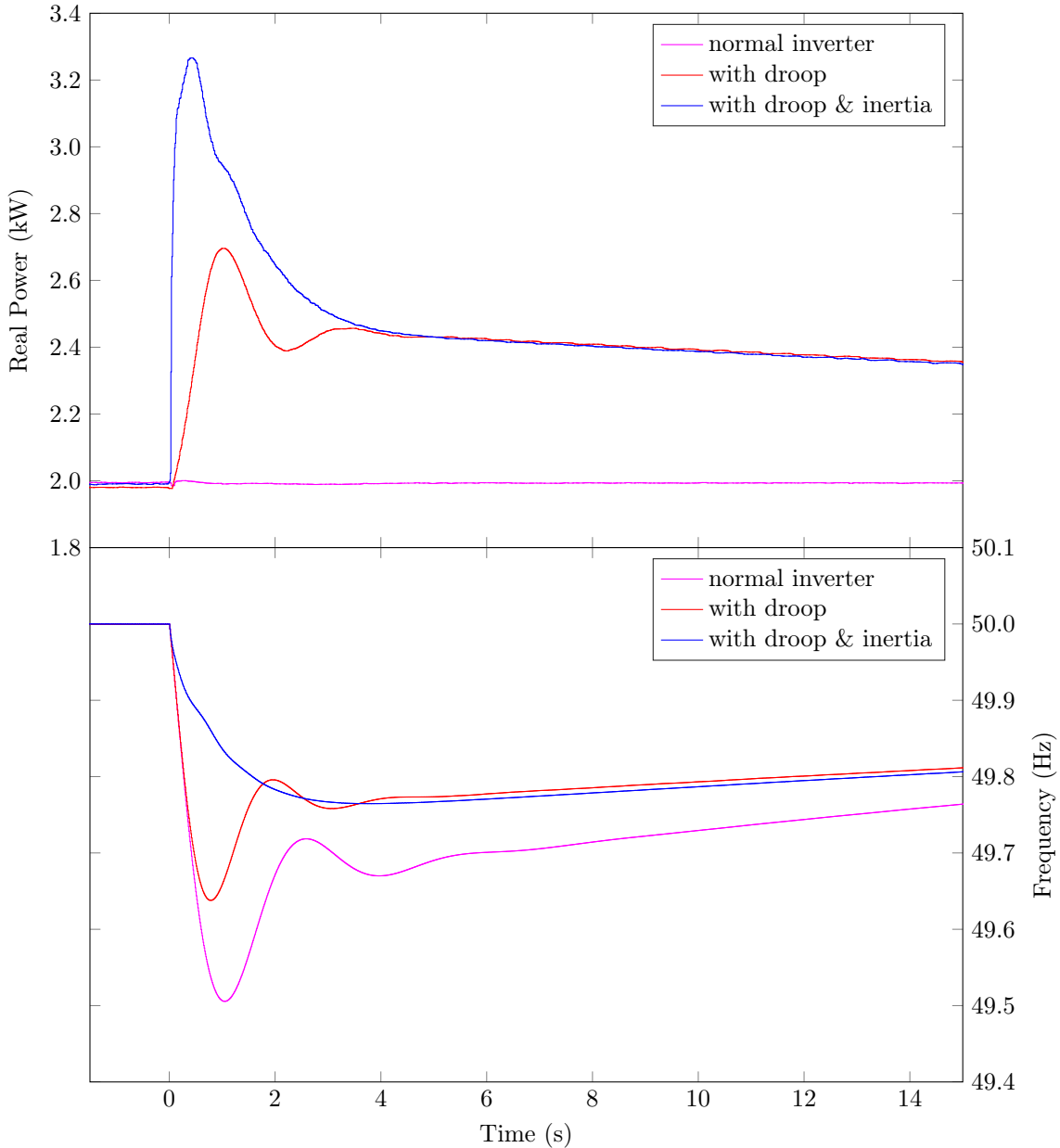


Figure 15: Simulation results confirming the effect of droop and virtual inertia on grid frequency. The upper subplot shows the inverter's output power, the lower subplot shows grid frequency. The addition of droop control reduces the magnitude of the frequency deviation, as does the addition of inertia emulation.

Part VI

Experimental Setup

VI.1 Overview

To test the response of the inverter to frequency deviations, it must be connected to a three phase network with a frequency that can be deliberately adjusted in a reproducible way. The local grid is not suitable, because its frequency deviations are rare and stochastic. Instead a programmable voltage supply was used. This supply can reproduce a pre-determined frequency deviation. It cannot react to the inverter's behaviour at runtime, so it cannot generate frequency curves such as those in Figure 15, which are generated based on the output of the inverter. Consequently the experimental testing does not aim to directly measure the impact of the VSM on grid frequency. Rather, the aim of the experimental testing is to confirm that the power output of the inverter during frequency deviations approximately matches that of the simulations, and of a real inertial machine. Section V.4 demonstrated that this behaviour does help reduce the speed and magnitude of frequency deviations. Therefore if the output power of the inverter matches that of simulations, then the experimental results will indirectly demonstrate that the implemented functionality helps regulate frequency.

Figure 16 shows the overall experimental setup. The programmable AC supply (*grid simulator*) produced frequency deviations. The real power output of the inverter during these deviations was measured with a power analyser, and compared to ideal inertia and droop. Photographs of the various components are shown in Figure 17.

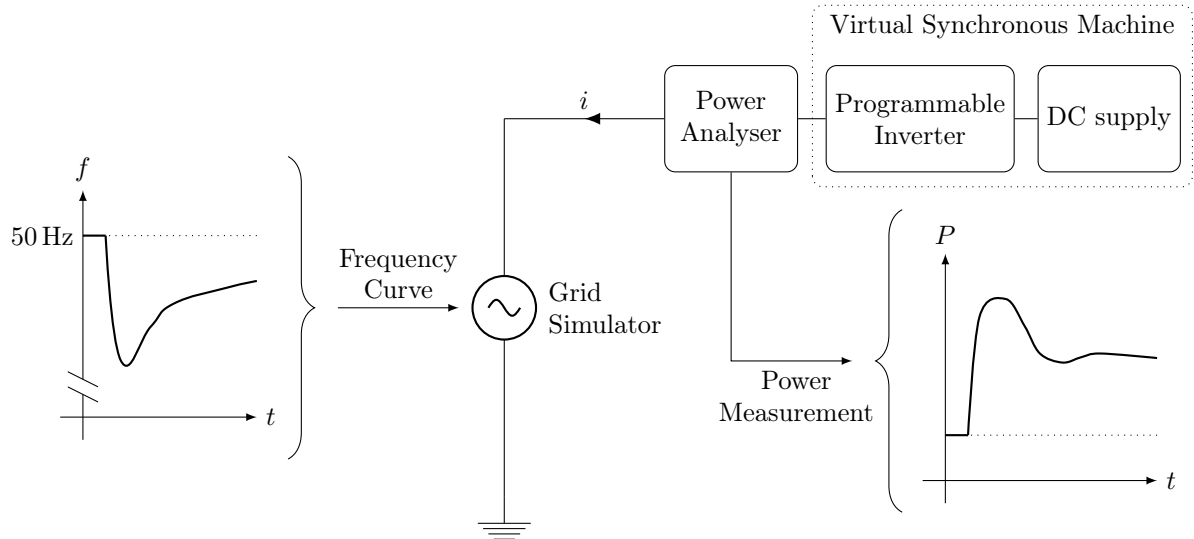


Figure 16: Schematic of experimental setup. The inverter was connected to an AC supply with programmable frequency, and a DC supply. The output power during frequency deviations was measured, and compared to an ideal generator with droop control and inertia.



(a) Regatron grid simulator (AC power supply)



(b) DC power supply



(c) Yokogawa WT3000 Power Analyser



(d) Creative Power 5 kVA Inverter

Figure 17: Photographs of the equipment used in the experimental setup.

VI.2 Inverter

The inverter used in this experiment is a 5 kVA, 3 phase, 2 level, 4 quadrant inverter made by Creative Power. The control code is written in C, which runs on TMS320F2810 DSP, programmed with a JTAG module. Some of the code was made available by the manufacturer, so that extra functionality such as inertia emulation can be added. The scope and detail of this programmability is described in Section IV.1.

The inverter uses an LC filter. The switching frequency and interrupt frequency are 10 kHz and 20 kHz respectively. The control system uses an PR current control loop. The outer PI DC voltage regulation loop has been replaced with a power control loop, as described in Section IV.2.

The operating mode, setpoint and other parameters can be manually modified during operation through a serial interface. This interface was also used for logging the inverter's internal measurements and parameters once per second.

VI.3 Grid Simulator

The AC supply is a Regatron ACS, 5 kVA, 3 phase *grid simulator*. This supply is a 4 quadrant voltage supply, with programmable frequency.

Ideally the VSM would be tested using frequency data from historical events. However the grid simulator lacks the necessary data import functionality. Instead the grid simulator can only generate relatively simple frequency deviations, such as ramps and sinusoids.

VI.4 DC Supply

If the AC voltage is at the nominal Australian voltage of 415 V (line to line), the inverter requires a DC voltage of between 700 V and 750 V.

The best DC supply available for this experiment is a TKD-Lambda supply which can provide up to 600 V. Consequently the DC supply was set to generate 600 V, and the AC supply was scaled down to $415 \text{ V} \times 600 \text{ V} \div 750 \text{ V} = 332 \text{ V}$ (line to line).

The DC supply can provide 25 A, which far exceeds the ratings of the inverter. The supply cannot sink current, so the experiment was restricted to only inverter mode (exporting power to the grid), and not rectifier mode (consuming power from the grid).

VI.5 Power Analyser

The power analyser used was a Yokogawa WT3000. Both the AC and DC sides were measured. The WT3000 has a bandwidth of 1 MHz, and logs measurement data twice per second.

VI.6 Protection and Isolation

Neither the DC supply nor the AC supply was isolated. Therefore an isolation transformer was needed somewhere in the circuit. It could either go in the AC line between the inverter and the AC supply, or it could go in the supply from the grid to the DC supply. The former would result in waveform distortion, so the latter was chosen. The isolation transformer used was a 3 phase, 5 kVA transformer, which matches the power rating of the inverter.

The earth terminals of all equipment (aside from the isolation transformer) were connected through the AC supply.

VI.7 Test Conditions

The reactive power output was set to 500 VAR for all tests included in this document. The nominal real power setpoint (upon which droop and inertial contributions are superimposed) was 2 kW for all tests included in this section. Appendix B on page 56 includes a test with a setpoint of 3.5 kW. Other real and reactive power setpoints were tested, but were excluded from this document for brevity. Equivalent results were observed for those tests.

A droop constant of 4% was used, because this is a typical value.

Typical synchronous machines have inertia constants (H) between 2 and 10 seconds [4]. The inertia constant used for inertia emulation calculations is not fixed, since it can be programmed to equal any value. An ideal grid has an infinite amount of inertia, so the programmed inertia constant should be as large as possible. If the programmed inertia constant is too large, the output power will saturate too easily, leading to a non-linear response which does not match real inertial machines.

If the apparent power setpoint is close to zero or rated power, the output will saturate easily for any amount of inertia. Consequently an inertial constant was chosen to suit an apparent power setpoint of 50%. The ROCOF threshold at which the inverter trips is 0.13 Hz/s. Substituting $\frac{df}{dt} = 0.13 \text{ Hz/s}$ and $P_{inertia} = 0.5S_n$ into Equation 9 on page 20 gives a maximum inertia constant of $H = 91 \text{ s}$. However during frequency deviations droop control will also be pushing the output power closer to saturation. Furthermore droop control tends to result in larger power deviations than inertial response. Consequently an inertial constant slightly less than half this value was chosen, which is $H = 40 \text{ s}$.

Most of the experimental tests were conducted without the directional inertia functionality described in Section IV.4. Such functionality was tested separately.

Part VII

Experimental Results

Unless stated otherwise, the following graphs were all created using independent measurements from the power analyser, not the inverter's internal measurements.

VII.1 Simple Frequency Deviation

VII.1.1 Frequency Waveform

The behaviour of the inverter was first tested with simple frequency deviations of both polarities, constructed with simple ramp functions. This frequency curve can be seen in the lower subplot of Figure 18. The specific values used to generate this frequency curve are included in Appendix A on page 55. These deviations are not realistic. However they were chosen because it is easy to visually confirm whether the qualitative shape of the output power matches the expected value.

Figure 18 shows the output power during these frequency deviations, for an inverter

- with droop control and inertia emulation both disabled;
- with droop control enabled and inertia emulation disabled; and
- with droop control and inertia emulation both enabled.

The output power is constant when droop control and inertia emulation are both disabled. This is as expected, since normal inverters are frequency agnostic. This output power approximately equals the setpoint of 2 kW. Therefore the power control loop sets the current setpoint correctly.

VII.1.2 Droop Control

In Figure 18 the output power when droop control is enabled is an inverted, scaled version of the frequency waveform, superimposed on the real power setpoint. This is as expected, since droop control should increase power output for low frequencies, and decrease it for high frequencies, by an amount proportional to the frequency deviation. Therefore the behaviour of the droop control is qualitatively correct.

Figure 19 on page 37 shows the output power when droop control is enabled and inertia emulation is disabled, and compares it to an ideal droop controlled generator, with the same amount of droop (4%). The maximum frequency in this test waveform is 50.75 Hz. For a 4% droop constant, a power setpoint of 2 kW and a rated power⁴ of 3977 VA, the maximum output power should be

$$P_{max} = 2000 + \frac{50.75 - 50}{50} \times 3977 \text{ VA} \div 0.04 \approx 3491 \text{ W} \quad (13)$$

⁴The rated current is 7.5 A, which corresponds to a lower power than the power rating, because the AC voltage is not at the nominal value. The rated current corresponds to $7.5 \text{ A} \times 3 \times 250 \text{ V} \div \sqrt{2} = 3977 \text{ VA}$.

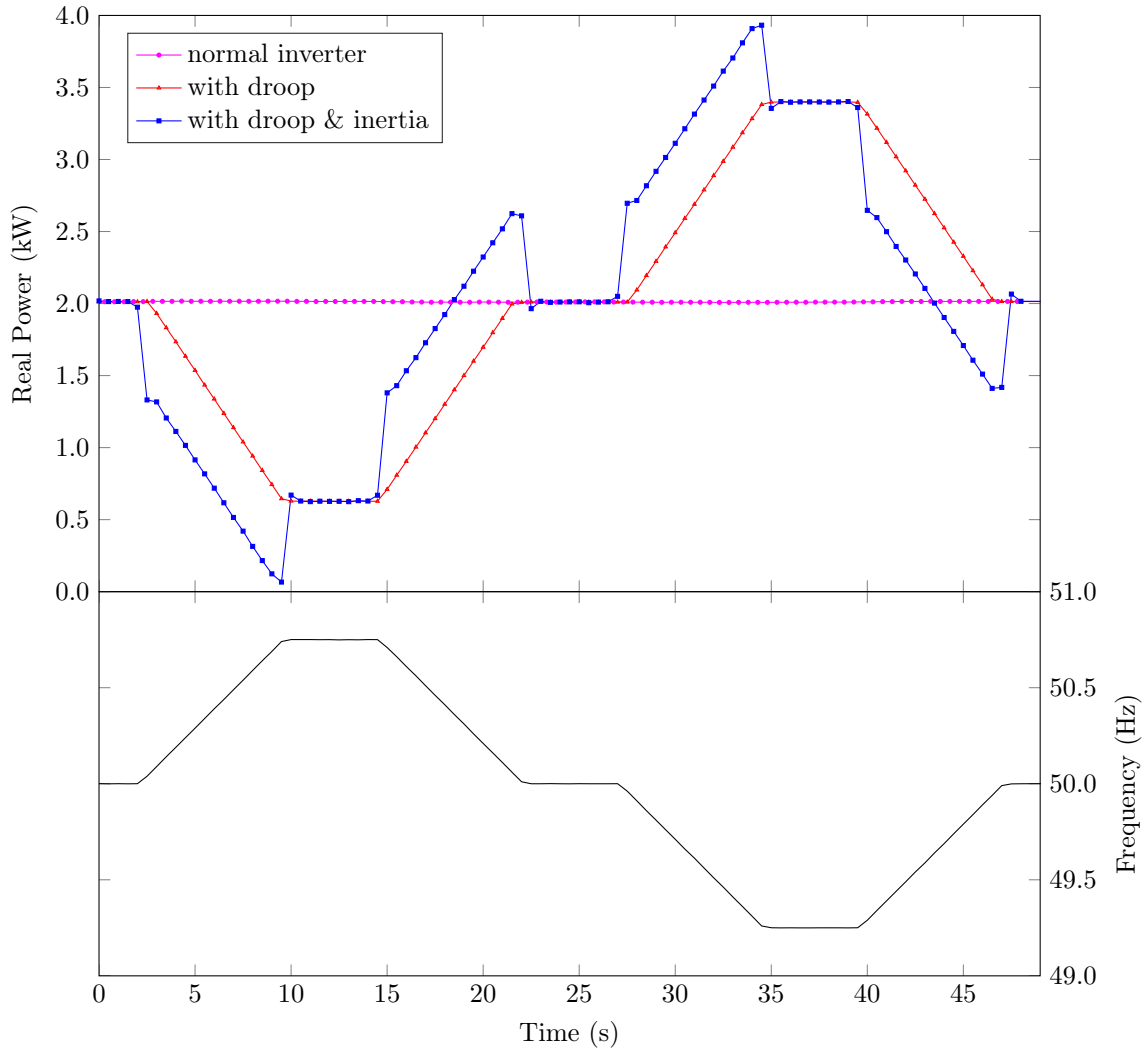


Figure 18: Experimental results showing the effect of droop and inertia emulation on output power (upper subplot) during simple frequency deviations (lower subplot). A normal inverter (pink) produces a constant power output. Droop control (red) subtracts an amount proportional to the frequency from the nominal power output. Inertia emulation (blue) subtracts an amount equal to the derivative of frequency from the power output.

The maximum measured value was 3401 W, which is very close to the theoretical value. Therefore the scaling of the droop control is correct.

The response time and propagation delay of the droop control is less than the 500 ms uncertainty of the time measurements. Therefore the speed of the droop control is sufficiently close to ideal.

Therefore Figure 19 demonstrates that the droop control works correctly.

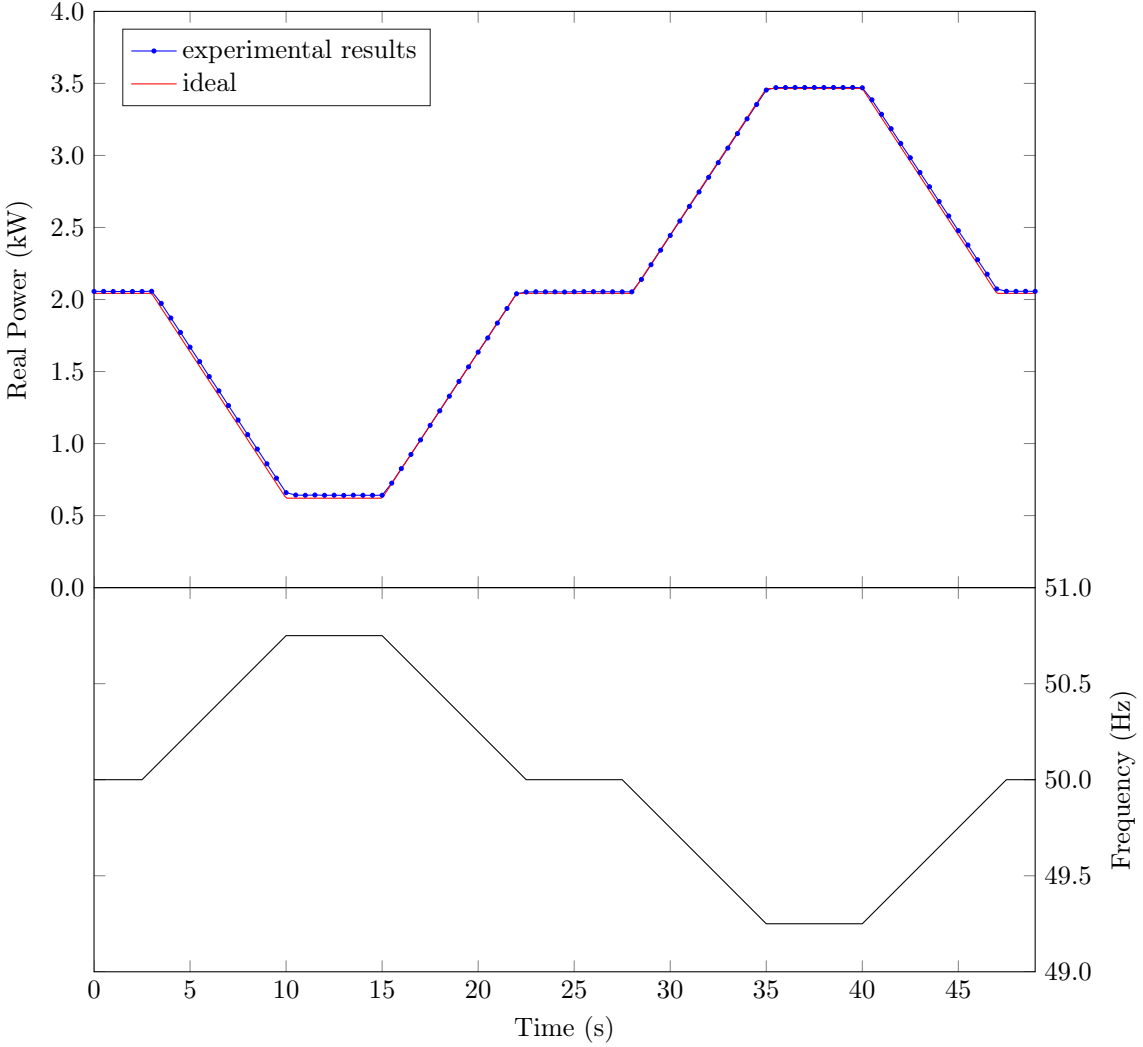


Figure 19: Comparison of experimental output power to ideal (upper subplot) during simple frequency deviations (lower subplot) with droop and without inertia. Droop control subtracts an amount proportional to the frequency from the nominal power.

VII.1.3 Inertia Emulation

The output power in Figure 18 when both droop control and inertia emulation is enabled is approximately as expected. That is, the blue curve in the upper subplot should be equal to the red curve, minus an amount proportional to the time derivative of frequency. The time derivative of the frequency waveform in the lower subplot is a simple 3 level wave. The difference between the blue and red curves in the upper subplot is approximately a 3 level wave. Therefore Figure 18 shows that the behaviour of

inertia emulation is qualitatively correct.

Figure 20 shows the real power output of the inverter with inertia emulation and without droop control, and compares it to an ideal inertial generator with real inertia (and without droop control). Droop control was disabled for this test to allow an independent assessment of the inertial response.

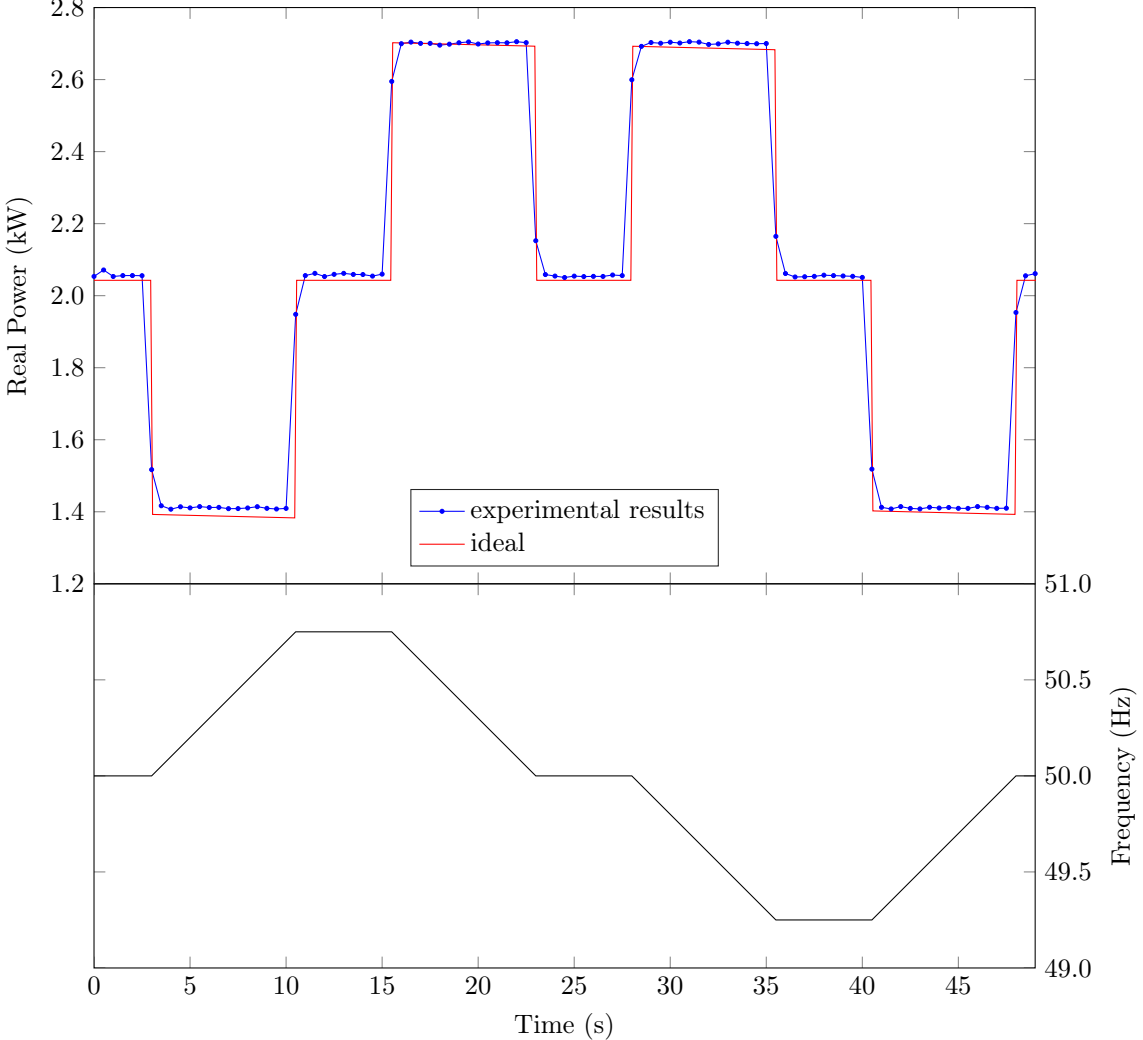


Figure 20: Comparison of experimental output power to ideal (upper subplot) during simple frequency deviations (lower subplot) with inertia and without droop. Inertia emulation subtracts an amount proportional to the derivative of frequency from the nominal real power output.

The frequency waveform rises and falls by 0.75 Hz in 7.5 s, which is a ROCOF of 0.1 Hz/s. For an inertia constant of $H = 40$ s, a real power setpoint of 2 kW, and a rated power of 3977 VA, Equation 9 on page 20 gives a maximum power of

$$P_{max} = 2 \text{ kW} + \frac{2 \times 40 \text{ s} \times 5 \text{ kW}}{50 \text{ Hz}} \times 0.1 \text{ Hz/s} \approx 2636 \text{ W} \quad (14)$$

The maximum measured output power was 2647 W, which is sufficiently close to the theoretical value. Therefore the scaling of the inertia emulation is correct.

The sample rate of the power analyser used for these results was 2 Hz, which was not fast enough to

accurately measure the propagation delay and rise time of the inertial response. This was measured separately with an oscilloscope. The results are presented and discussed in Section VIII.4 on page 47. When examining the transients in Figure 20 note the location of the specific sample points, which are far more ideal than the lines between the points imply.

Figure 21 shows the output power of the inverter with both droop control and inertia emulation enabled, and compares it to the ideal value. The scaling of the output power closely matches the ideal values, which is as expected since it was demonstrated above that droop control and inertia emulation each work separately. The main difference between the ideal and observed power output is the aforementioned inertial response rise time, which is discussed in Section VIII.4.

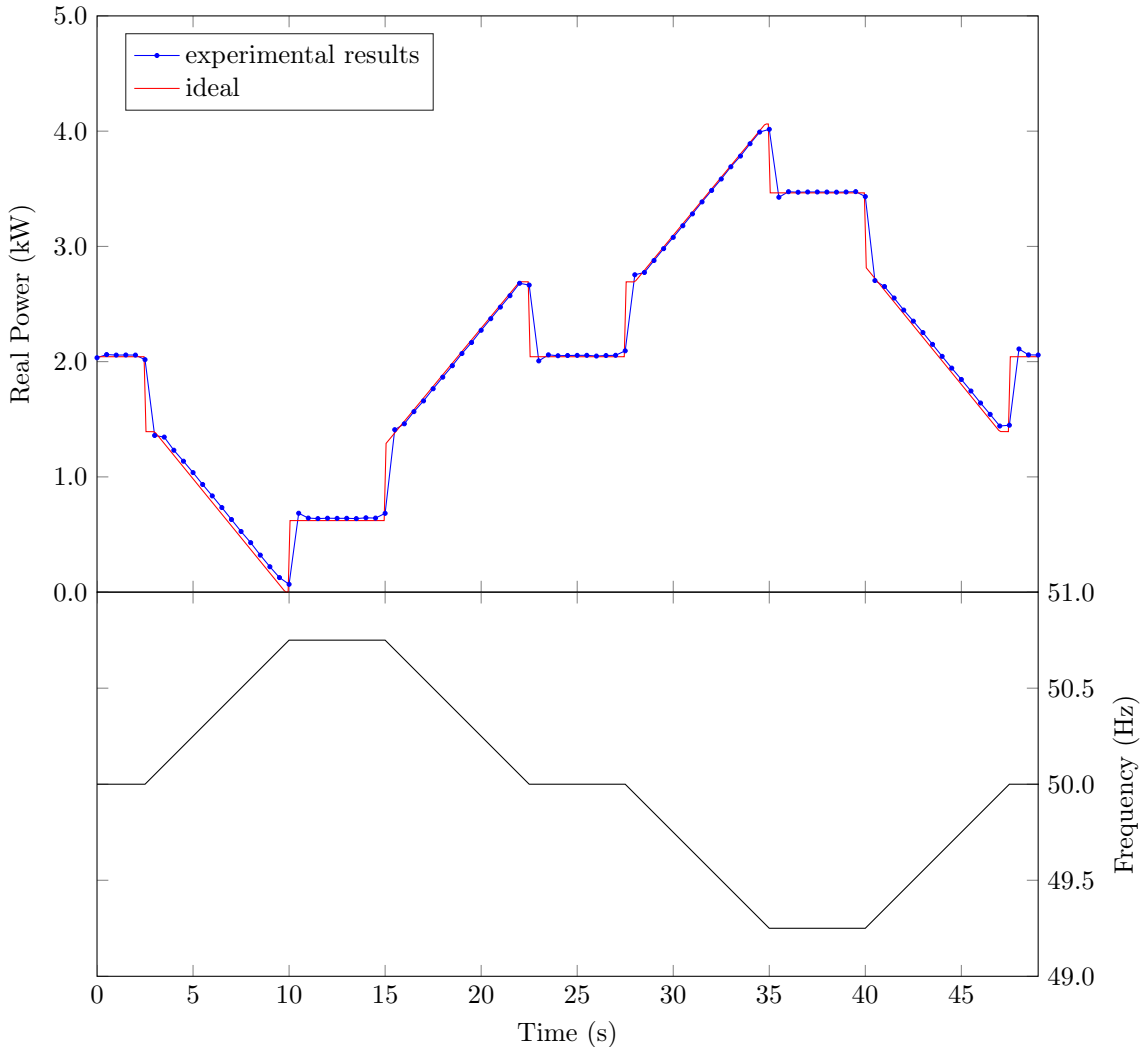


Figure 21: Comparison of experimental output power to ideal (upper subplot) during simple frequency deviations (lower subplot) with droop and inertia.

Therefore Figure 21 demonstrates that the droop control and inertia emulation works correctly, aside from the lag.

VII.2 Realistic Frequency Deviation

VII.2.1 Frequency Waveform

As mentioned in Section VI.3, the grid simulator cannot import data from historical frequency deviations, so it is unable to reproduce such curves exactly. Instead a series of ramps was used to construct a fictional curve approximating a typical under frequency deviation. This frequency curve can be seen in the lower subplot of Figure 22. The specific values used to generate this frequency curve are included in Appendix A on page 55.

The grid simulator has a limit on the number of data points which can be used to construct such a curve. Consequently over frequency and under frequency events needed to be tested separately. The inverter responded equivalently for under frequency and over frequency events. For brevity only under frequency events have been included in this section. The results for over frequency deviations are included in Appendix B on page 56.

VII.2.2 Impact of Droop and Inertia

Figure 22 shows the output power during these frequency deviations, for an inverter

- with droop control and inertia emulation both disabled;
- with droop control enabled and inertia emulation disabled; and
- with droop control and inertia emulation both enabled.

As expected, the power output of the inverter without droop control or inertia emulation is constant. Also as expected, the output power when droop control is enabled is an inverted, scaled version of the frequency waveform, superimposed on the real power setpoint. The addition of inertia emulation results in a higher output power during the outwards frequency swing, and lower during the inwards swing. In particular the rise time of the power immediately after the deviation commences is higher with inertia. This is as expected, since it is this early injection of extra power which makes inertia so important and useful. Therefore the behaviour of droop control and inertia emulation is qualitatively correct.

Figure 23 shows the output power of the inverter with both droop control and inertia emulation enabled, and compares it to an ideal generator. The difference between the measured and ideal values mostly corresponds to the error in the estimate of ROCOF, which is shown in the lower subplot of Figure 23.

The lower subplot of Figure 23 appears to show a slow fall time for the inverter's estimate of ROCOF. However it should be noted that due to the low sample rate of the inverter serial output (1 Hz), the slope appears more horizontal than it probably is. There is only one sample along the initial fall, which means the fall time could be very small. It is very difficult to increase this sample rate. Since these are internal values, no external instrumentation can be used. Logging high sample rate data to memory during the event and slowly exporting it through the serial interface afterwards was considered. However due to the limited memory space this was not possible. The speed of the output power response was measured at a higher sample rate, which gives an indication of the speed of the ROCOF estimate. Those results are shown in the following section.

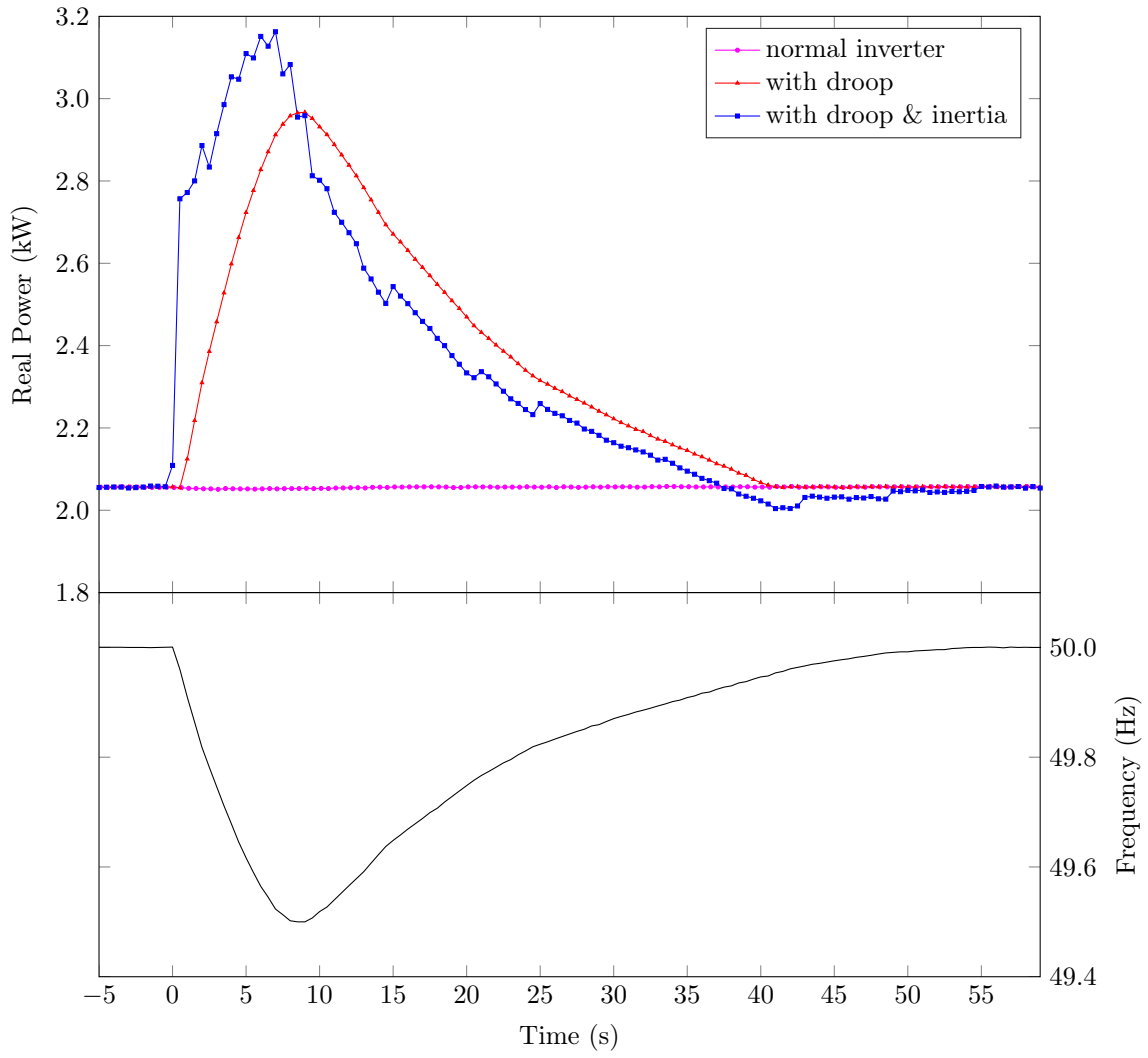


Figure 22: Experimental results showing the effect of droop and inertia emulation on output power (upper subplot) during a realistic under frequency deviation (lower subplot). A normal inverter (pink) produces a constant power output. Droop control (red) subtracts an amount proportional to the frequency from the nominal power output. Inertia emulation (blue) subtracts an amount equal to the derivative of frequency from the power output.

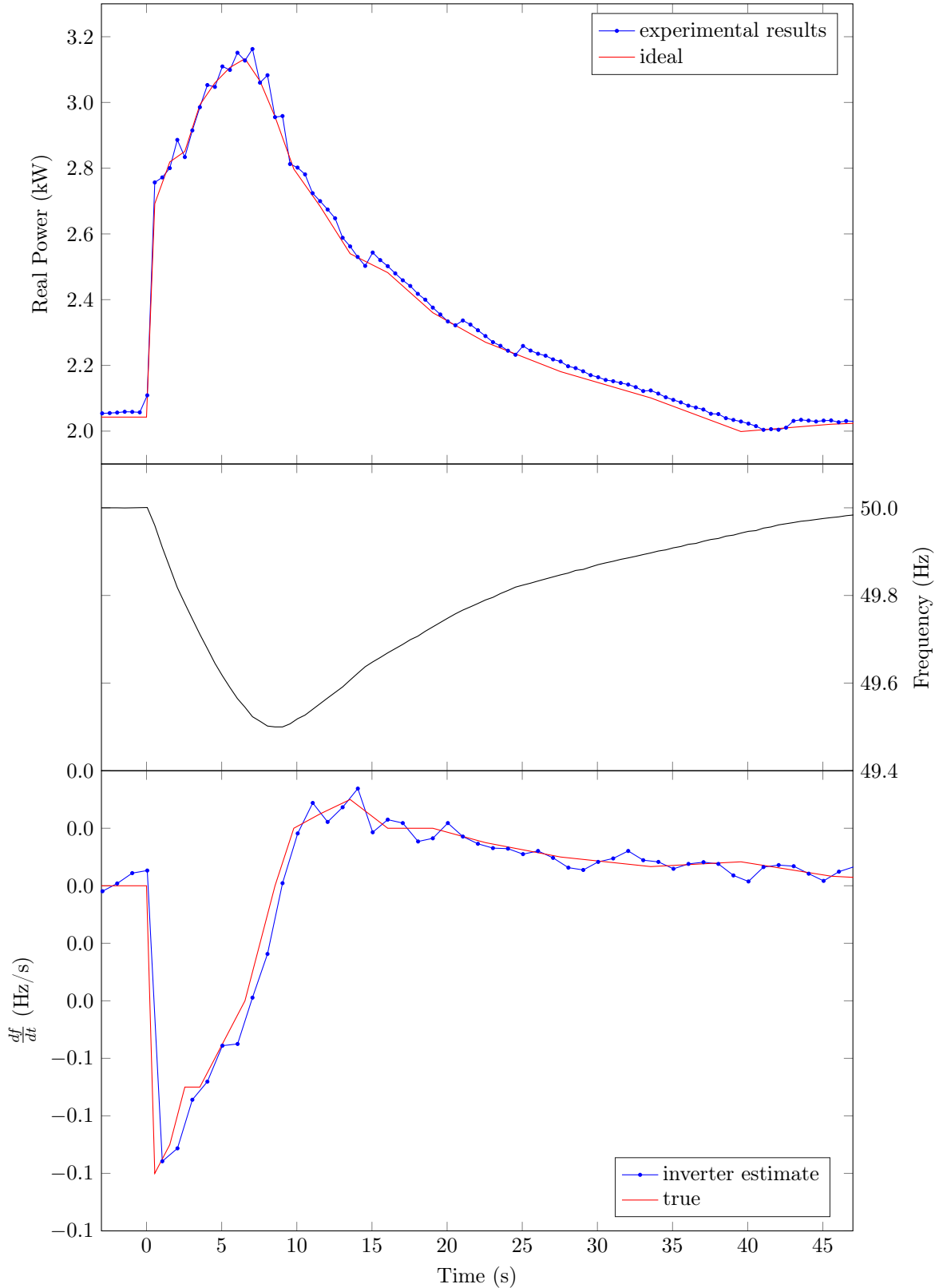


Figure 23: Experimental results showing the effect of droop and inertia emulation during a realistic under frequency deviation. The top subplot compares the inverter power output to a conventional generator with droop control and real inertia. The inverter's estimate of frequency and its derivative is compared to the true value in the middle and bottom subplots respectively.

Therefore Figure 23 shows that the VSM works as it was designed to.

VII.3 Inertia Emulation Speed

When the grid frequency was transitioned from a constant value to a ramp of 0.1 Hz/s, the propagation delay and rise time were measured to be 200 ms and 255 ms respectively. This response is shown in Figure 24, where inertia emulation is enabled and droop control is disabled. The small phase imbalance seen in the middle subplot of Figure 24 is due to imperfections in the pre-existing current control loop, which could not be improved for this thesis. It is not due to the inertia emulation.

VII.4 Directional Inertia

The directional inertia functionality described in Section IV.4 on page 21 was implemented and tested using the simple frequency waveform described in Section VII.1.1. Figure 25 shows the power output of an inverter

- with droop control and inertia emulation both disabled;
- with droop control enabled and inertia emulation disabled; and
- with droop control and inertia emulation both enabled.

Figure 25 shows that the code successfully disables the inertial response during the return swing of frequency, which is the intended behaviour. Therefore directional inertia was successfully implemented. The usefulness and limitations of this behaviour is discussed further in Section VIII.5 on page 48. The directional inertia reacts slower only because the direction sensing uses a deadband on the frequency measurement.

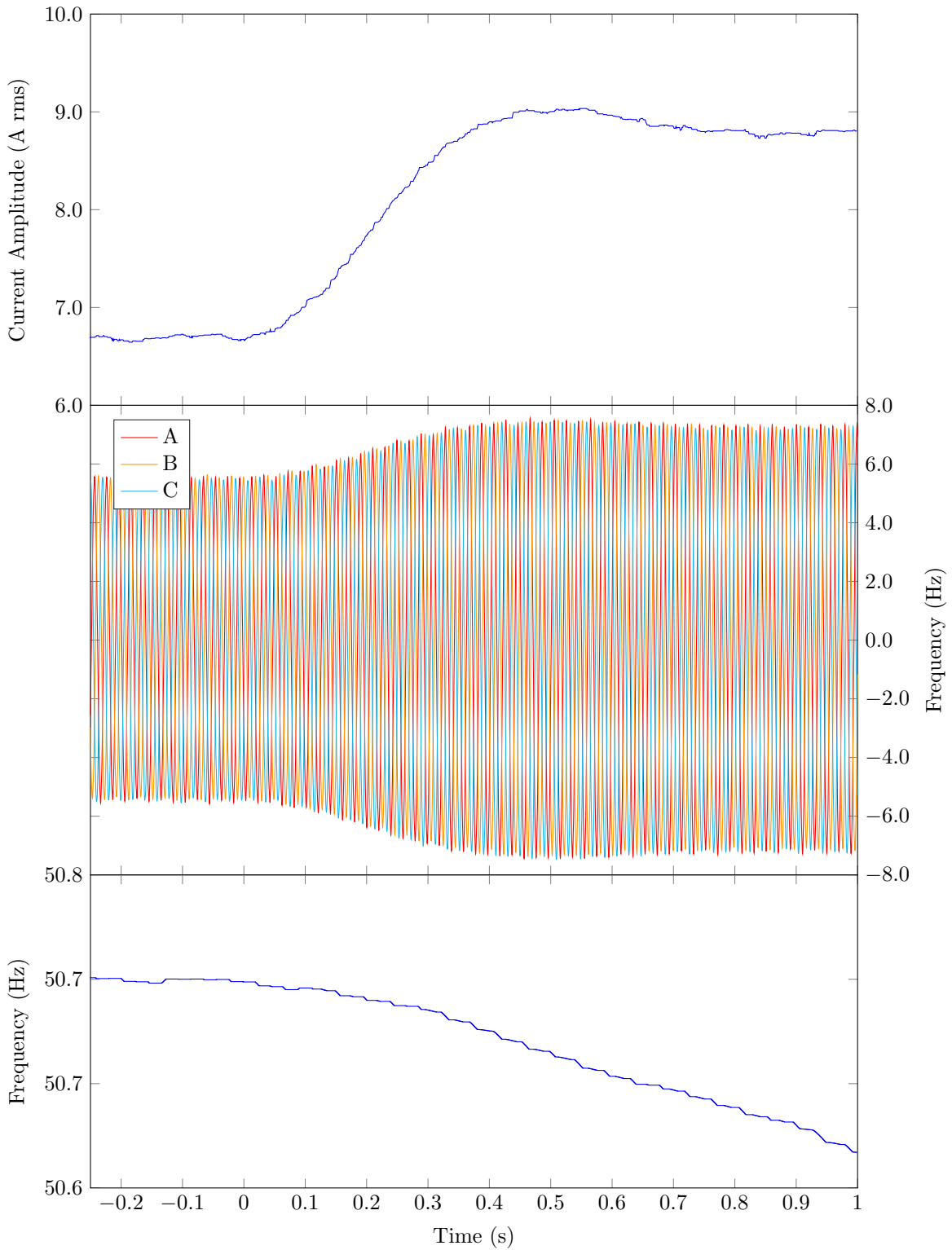


Figure 24: Overall propagation delay and rise time of inertial response. The frequency transitions from constant to a downwards ramp at 0 s (lower subplot). The output current magnitude and sinusoids are shown in the top and middle subplots respectively. The small phase imbalance in the middle subplot is due to pre-existing imperfections in the current control loop, and not the inertia emulation.

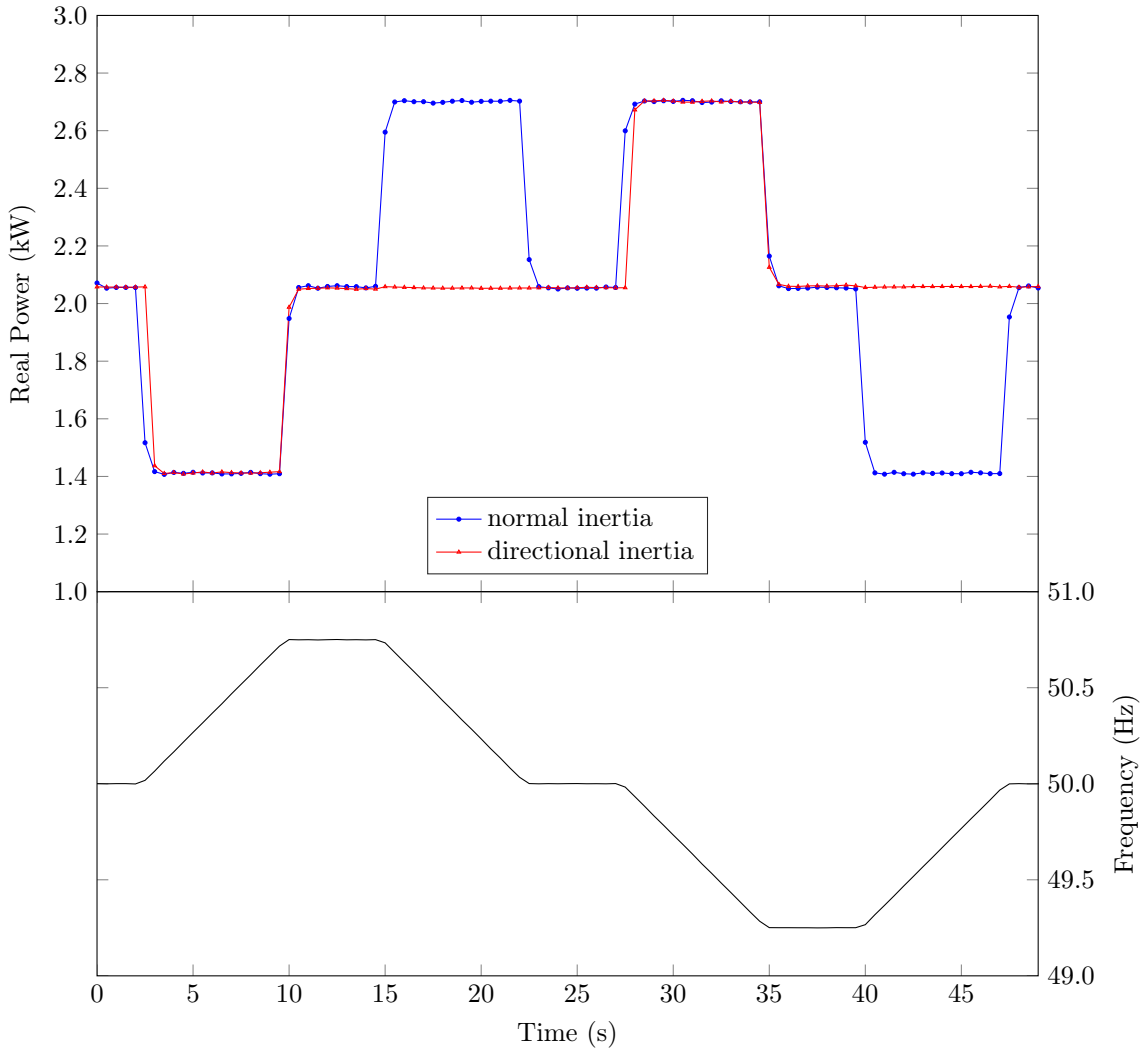


Figure 25: Comparison of normal inertia (blue) and ‘directional’ inertia (red). With directional inertia the scaled derivative of frequency is only subtracted from the power output (upper subplot) when the frequency is deviating away from nominal, and not back towards it (lower subplot). The directional inertia reacts slower only because the direction sensing uses a deadband on the frequency measurement.

Part VIII

Discussion

VIII.1 Results Summary

The experimental results demonstrated that droop control and inertia emulation were implemented successfully, and that the system works as intended. Therefore the aim of this thesis has been satisfied. The only notable shortcoming of is that of the lag in inertial response. The cause and acceptability of this lag is discussed in Section VIII.4.

The power output when inertia emulation was enabled was less smooth than the ideal curve. This is mostly caused by imperfect filtering of the frequency measurement both before and after the time derivative operation. Taking the derivative of a signal necessarily exacerbates the high frequency noise components. The output power could be further smoothed with more intense filtering, however this would compromise the response time. The amount of high frequency oscillation seen in the output power in the results is acceptable, since these oscillations would be mostly uncorrelated between different inverters (particularly those of different make and model), thereby cancelling out.

For some tests (such as Figure 20 on page 38) there was a slight gain error and offset error between the ideal values and the experimental results. These errors are probably caused by rounding errors in the fixed point computations, and imperfect calibration of the inverter's analog to digital converter. These errors are acceptable, since they would vary between different makes and models of inverters, thereby cancelling out. Furthermore, a small gain error in the inertia emulation system would be acceptable, since the inertia constant used in this experimental test is already many times higher than for conventional generators.

VIII.2 Polarity

The DC supply used in the experimental testing was not able to sink current. Consequently the inverter was only tested while nominally exporting power to the grid (discharging the battery), and not while importing power from the grid (charging the battery). There is no reason to expect that the droop control and inertial emulation performance will be different between importing and exporting.

As a consequence of the mathematics, if an over frequency event is fast and large enough, the droop and inertial contributions to power output may be large enough to cause the real power output to become negative whilst the battery is nominally discharging. The saturation block described in Section IV.7 saturates the transient real power output (including droop control and inertia emulation) to prevent this, solely because the DC supply cannot sink current. However a battery's power electronics should be able to switch seamlessly between charging and discharging, so the lower saturation limit should be -100%, not 0% of real rated power output. It is likely however that such polarity changes may wear the battery if they are too frequent, thereby reducing the performance and lifespan of the battery. An analysis of the impact of inertia emulation on a battery's chemical wellbeing is beyond the scope of this thesis.

VIII.3 Upper Inertia Limit

As discussed in Section VI.7 on page 34, the inertia constant H can be chosen freely, since it is defined only in software. A constant of 40 s was chosen for the experimental testing, which is at least 4 times larger than that of a typical inertial generator. This means that a VSM can contribute a far larger inertial response than conventional generators. However there are two caveats to such a comparison. The first is the non-zero response time discussed in Section VIII.4.1.

The second is that if the chosen inertia constant is very large, the power output will saturate easily during large and fast frequency swings. Once this happens, the response no longer matches that of a real inertia with the same inertia constant. Rather, the effective inertia constant is reduced during the saturation period. If the inverter's nominal real power setpoint is close to the rated power, upper saturation will occur during under frequency deviations even with small inertia constants. Experimental tests demonstrating this behaviour are included in Appendix B on page 56. This does not happen with real synchronous machines.

VIII.4 Speed of Inertial Response

VIII.4.1 Issue

The power contributions from inertial responses are most critical immediately after an event. Real inertia reacts instantaneously. Inertia emulation necessarily has an associated delay, inherent in the measurement, detection and actuation stages.

VIII.4.2 Causes

As shown in Section VII.3 on page 43, the inertia emulation system developed in this thesis has a propagation delay and rise time of 200 ms and 255 ms respectively. The contributors to the overall system lag are

- The error with which a non-ideal PLL tracks frequency;
- The step response of the low pass IIR filter used to smooth the output of the PLL;
- The step response of the rolling mean used to smooth the derivative of frequency;
- The speed of the inner current control loop; and
- The inherent time required to change the current in the LC filter using a finite DC supply.

The lag associated with the hardware and the inner current control loop were determined through experimental measurements. The remaining lags were estimated through simulation. It was found that the delay introduced by the IIR filter was large enough to make all other sources of lag negligible.

The IIR filter is necessary for smoothing out the measurement of frequency. Without it the output of the droop and inertia stages would be erratic. When taking the derivative of frequency to calculate the inertial response, high frequency noise is exacerbated. Frequency filtering removes this noise prior to the derivative calculation. Without any filtering the resulting inertia emulation would be too erratic to be of any use, and may even compromise the stability of the inverter control system.

Further work should be undertaken to develop a higher performance filter and PLL. Most of the frequency estimate noise comes from the PLL itself, and not the raw voltage measurements. In addition to co-optimising delay and output smoothness, any new filter must also adhere to the execution time and memory space constraints of the inverter.

VIII.4.3 Requirements

The time within which inertia emulation must react is limited by the maximum rated ROCOF and the bounds of the allowable frequency band. The former is set by the maximum contingency size, and the amount of real inertia in the network.

For example AEMO normally operates such that any credible contingency in South Australia would result in at most a 1 Hz/s ROCOF [28]. The lower frequency bound for a credible contingency in South Australia is at most 49.5 Hz. Therefore the frequency after a typical credible contingency could become unacceptable within $(50 \text{ Hz} - 49.5 \text{ Hz}) \div 1 \text{ Hz/s} = 500 \text{ ms}$. Inertia emulation must react within this time window in order to help prevent unacceptable frequency deviations. The experimental results in this thesis show that inertia emulation can become 10% and 90% actuated, within approximately 80 ms and 330 ms respectively. Therefore the response time of the system developed in this thesis is sufficient to be of use in such a case.

The maximum credible ROCOF is a soft constraint. For example Ireland's grid currently has a maximum credible ROCOF of 0.5 Hz/s, but is transitioning to 1 Hz/s [28]. The interconnectors to South Australia are typically operated to constrain the ROCOF after the largest credible contingency to within 1 Hz/s, however under frequency load shedding is designed to operate at up to 3 Hz/s, and generators should remain online for ROCOFs of up to 4 Hz/s for up to 0.25 s [28, 29]. Immediately prior to the state-wide outage in South Australia in September 2016, the ROCOF exceeded 6 Hz/s [29].

Similarly, the lower allowable frequency is hard to specify. For example in the NEM the absolute lower frequency bound of 47 Hz could be used for calculations instead of the generation or load contingency bound of 49.5 Hz.

Calculating the maximum reaction time for inertia emulation is straightforward for given ROCOF and frequency limits. However choosing such limits is difficult. As mentioned above, the system developed in this thesis can react fast enough to assist after most credible contingencies in the NEM.

VIII.5 Directional Inertia

Section IV.4 on page 21 discussed the motivation and definition of directional inertia. The experimental results confirmed that directional inertia can be successfully implemented. Directional inertia should hasten the return to nominal frequency after an excursion, which is desirable. However it does so by increasing the ROCOF on the return swing. If too much inertia is disabled on the return swing, the increase in ROCOF may be too high. Furthermore, this behaviour may introduce stability issues. An analysis of the trade off between improving frequency restoration at the expense of higher ROCOF, and of the stability impact of directional inertia is beyond the scope of this thesis. In this thesis directional inertia was conceived, and verified only on a per-device level.

VIII.6 Commercial Value and Industry Significance

These experimental results prove that it is possible to control an inverter to mimic the inertial behaviour or conventional generators. In particular the reaction time can be short enough for the system to provide material support to grid frequency immediately after most network events, such as the tripping of a generator or interconnector.

Transitioning to very high penetration levels of renewables is crucial for addressing climate change. The issue of low inertia is currently one of the largest obstacles to achieving this transition. Ireland and the French Islands are already spilling cheap and clean renewable energy in favour of fossil fuels because of this inertia issue [11, 15]. There exists a need in the Australian electricity industry (and globally) to address the issue of low inertia whilst simultaneously reducing emissions. The inertia emulation control system implemented in this thesis meets this need. Inertia emulation does have some limitations and non-ideal characteristics. However the experimental and simulation results in this thesis demonstrate that it is possible to implement inertia emulation with batteries well enough to help address low inertia issues.

As discussed in Section II.1.6.3 on page 13, inertia emulation provides a material benefit to the electricity market. Incentives such as inertia markets should be put in place to incentivise inverter manufacturers to implement control systems such as that which is described in this thesis [16, 17]. This is necessary to overcome the cost of adding the complexity of such a system to the inverter design.

Furthermore, there exist regulations which prohibit the use of inertia emulation for ordinary frequency regulation (as opposed to reacting to contingencies). If such regulations are removed, this technology would become more commercially viable.

The inertia emulation algorithm implemented in this thesis requires only local measurements. This autonomy means that there is no need to construct costly communications infrastructure, nor administer a dispatch system. Consequently, small generation aggregators will face relatively few barriers to entry when they start trying to commercialise inertia emulation.

Part IX

Conclusion

IX.1 Results

In this thesis the control system of a 5 kVA, 3 phase programmable inverter was modified to mimic the behaviour of conventional droop controlled generators with physical inertia. The additional code now controls the output real power to be equal to a nominal power setpoint, minus an amount proportional to the frequency deviation from 50 Hz (droop control), minus an amount proportional to the derivative of frequency (inertia emulation). An inverter with such functionality is called a virtual synchronous machine (VSM). The purpose of this functionality is to minimise the speed and magnitude of frequency deviations in a grid with low levels of inertia.

This system was experimentally tested by connecting the inverter to a DC power supply to mimic an ideal battery, and also to a programmable AC supply representing the grid, which reproduced a variety of frequency deviations. The experimental results showed that the inverter was able to closely match the power output of an ideal generator with droop control and real inertia. It was experimentally demonstrated that the inverter can emulate inertia constants of up to 40 s, which is several times larger than conventional generators. Simulation results demonstrated that such a response does reduce the speed and magnitude of frequency deviations on the grid.

The main discrepancy between the experimental results and ideal results is the non-zero propagation delay and rise time of the inertial response. The propagation delay and rise time were measured to be 200 ms and 255 ms respectively. This lag is sufficiently short that such an inertial response would be useful for most credible contingencies in the NEM.

In summary, the objectives of this thesis have been achieved.

IX.2 Key Contributions

- Droop control and inertia emulation were successfully implemented and experimentally tested on a battery inverter. The inertia emulation is fast enough to be useful during most credible contingencies in the NEM.
- A computationally efficient, fixed point PLL and subsequent filtering system was developed, in order to satisfy the unique and stringent frequency measurement constraints necessary for a smooth yet rapid inertial response.
- An accurate and fast Simulink model of the specific inverter used in the experimental testing was produced, which incorporates the exact C code used in the real system.
- Improvements to the average switching model of inverter PWM switching, to allow simulation of the DC side of the switches, including soft charging at startup, and also to model saturation more accurately.
- An innovative *directional inertia* was proposed, implemented and experimentally verified. Real inertia opposes changes to frequency even when that change is the desired change back to nominal

after a deviation. With directional inertia the inertial contribution is disabled when frequency is changing towards nominal. This should hasten the return of frequency to nominal after a deviation, although there are some drawbacks which require further investigation.

IX.3 Future Work

- For completeness, future work on this topic should experimentally test the behaviour of VSMs whilst importing power from the grid.
- The AC supply used in this thesis was not able to calculate a frequency at runtime based on the behaviour of the inverter. Future work should include testing a VSM with a responsive AC supply or real synchronous generators, in order to experimentally verify that the inertial response achieved in this thesis does indeed reduce the speed and magnitude of frequency deviations.
- As mentioned in Section VIII.4.2, future work should be conducted to improve the filters applied to the frequency measurement, to maximise output smoothness whilst minimising propagation delay, rise time and computational cost.
- The scope of this thesis was restricted to regulating grid frequency. Future research should implement voltage ($Q-V$) droop, to help regulate grid voltage as well as frequency.
- Research should be undertaken to determine how significantly the power output deviations of a VSM would reduce the lifespan and capabilities of the battery itself. In particular it should be investigated whether or not the polarity reversals described in Section VIII.2 would significantly wear the battery.
- As mentioned in Section VIII.5, future work should investigate whether the benefits of the directional inertia proposed in this thesis outweigh the disadvantages.
- A discussion of the financial viability and possible market incentives for inertia emulation is beyond the scope of this thesis. Future work should include such an investigation.

Bibliography

- [1] W. Phipps, M. J. Harrison, and R. M. Duke, “Three-phase phase-locked loop control of a new generation power converter,” in *Industrial Electronics and Applications, 2006 1ST IEEE Conference on*. IEEE, 2006, pp. 1–6. [Online]. Available: <http://www.ir.canterbury.ac.nz/handle/10092/1924>
- [2] A. D. Paquette, “Power quality and inverter-generator interactions in microgrids,” Ph.D. dissertation, Georgia Institute of Technology, Jan. 2014. [Online]. Available: <http://hdl.handle.net/1853/51803>
- [3] J. Machowski, J. Bialek, and J. Bumby, *Power System Dynamics and Stability*. Wiley, 1997.
- [4] A. Ulbig, T. Borsche, and G. Andersson, “Impact of low rotational inertia on power system stability and operation,” *arXiv*, Dec. 2014. [Online]. Available: <http://arxiv.org/abs/1312.6435>
- [5] “100 per cent renewables study - modelling outcomes,” Australian Energy Market Operator, Tech. Rep., Jul. 2013. [Online]. Available: <http://www.environment.gov.au/system/files/resources/d67797b7-d563-427f-84eb-c3bb69e34073/files/100-percent-renewables-study-modelling-outcomes-report.pdf>
- [6] A. Ulbig, T. Rinke, S. Chatzivasileiadis, and G. Andersson, “Predictive control for real-time frequency regulation and rotational inertia provision in power systems,” in *2013 IEEE 52nd Annual Conference on Decision and Control (CDC)*, Dec. 2013, pp. 2946–2953.
- [7] S. Sharma, S.-H. Huang, and N. Sarma, “System inertial frequency response estimation and impact of renewable resources in ERCOT interconnection,” in *Power and Energy Society General Meeting, 2011 IEEE*. IEEE, Jul. 2011, pp. 1–6. [Online]. Available: http://ieeexplore.ieee.org/xpl/login.jsp?tp=&arnumber=6038993&url=http%3A%2F%2Fieeexplore.ieee.org%2Fxpls%2Fabs_all.jsp%3Farnumber%3D6038993
- [8] N. R. Ullah, T. Thiringer, and D. Karlsson, “Temporary primary frequency control support by variable speed wind turbines—potential and applications,” *IEEE Transactions on Power Systems*, vol. 23, no. 2, pp. 601–612, May 2008.
- [9] J. Morren, S. de Haan, and J. Ferreira, “Contribution of DG units to primary frequency control,” *European Transactions on Electrical Power*, vol. 16, no. 5, pp. 507–521, Nov. 2006. [Online]. Available: <http://dx.doi.org/10.1002/etep.113>
- [10] L. Miao, J. Wen, H. Xie, C. Yue, and W.-J. Lee, “Coordinated control strategy of wind turbine generator and energy storage equipment for frequency support,” *IEEE Transactions on Industry Applications*, vol. 51, no. 4, pp. 2732–2742, Jul. 2015.
- [11] P. Tielens and D. Van Herrem, “Grid inertia and frequency control in power systems with high penetration of renewables,” in *Young Researchers Symposium in Electrical Power Engineering*. KU Leuven Association, Apr. 2012. [Online]. Available: <https://lirias.kuleuven.be/handle/123456789/345286>
- [12] “Market ancillary service specification,” Australian Energy Market Operator, Tech. Rep., May 2012.
- [13] “Response of existing PV inverters to frequency disturbances,” Australian Energy Market Operator, Tech. Rep., Apr. 2016.

- [14] *Grid connection of energy systems via inverters*, Standards Australia Std. AS 4777, 2005.
- [15] *Design and Operating Requirements for the Connection of Power Generation Facilities to MV or LV Distribution Grids*, French Ministerial Order Std. DEVE0 808 815A, Apr. 2016. [Online]. Available: <https://www.legifrance.gouv.fr/affichTexte.do?cidTexte=JORFTEXT000018698004>
- [16] General Electric International, Inc., “Frequency response study,” California ISO (CAISO), Tech. Rep., Nov. 2011.
- [17] E. Muljadi, V. Gevorgian, M. Singh, and S. Santoso, “Understanding inertial and frequency response of wind power plants,” in *IEEE Symposium on Power Electronics and Machines in Wind Applications*. Denver, Colorado: IEEE, Jul. 2012.
- [18] S. Nanou, A. Papakonstantinou, and S. Papathanassiou, “A generic model of two-stage grid-connected PV systems with primary frequency response and inertia emulation,” *Electric Power Systems Research*, vol. 127, pp. 186–196, 2015. [Online]. Available: <http://www.sciencedirect.com/science/article/pii/S0378779615001868>
- [19] M. Torres and L. Lopes, “Frequency control improvement in an autonomous power system: An application of virtual synchronous machines,” in *IEEE 8th International Conference on Power Electronics - ECCE Asia (ICPE & ECCE)*. IEEE, May 2011, pp. 2188–2195.
- [20] M. R. Aghamohammadi and H. Abdolahinia, “A new approach for optimal sizing of battery energy storage system for primary frequency control of islanded Microgrid,” *International Journal of Electrical Power & Energy Systems*, vol. 54, pp. 325–333, 2014. [Online]. Available: <http://www.sciencedirect.com/science/article/pii/S0142061513003025>
- [21] T. Borsche, A. Ulbig, M. Koller, and G. Andersson, “Power and energy capacity requirements of storages providing frequency control reserves,” in *IEEE PES General Meeting, Vancouver*, Jul. 2013, pp. 1–5. [Online]. Available: https://www.eeh.ee.ethz.ch/uploads/tx_ethylpublications/borsche_GM_2013.pdf
- [22] I. Serban and C. Marinescu, “Battery energy storage system for frequency support in microgrids and with enhanced control features for uninterrupted supply of local loads,” *International Journal of Electrical Power & Energy Systems*, vol. 54, pp. 432–441, 2014. [Online]. Available: <http://www.sciencedirect.com/science/article/pii/S0142061513003013>
- [23] M. Torres, L. Lopes, L. Morán, and J. Espinoza, “Self-tuning virtual synchronous machine: A control strategy for energy storage systems to support dynamic frequency control,” *IEEE Transactions on Energy Conversion*, vol. 29, no. 4, pp. 833–840, Dec. 2014.
- [24] G. Delille, B. Francois, and G. Malarange, “Dynamic frequency control support by energy storage to reduce the impact of wind and solar generation on isolated power system’s inertia,” *IEEE Transactions on Sustainable Energy*, vol. 3, no. 4, pp. 931–939, Oct. 2012. [Online]. Available: http://ieeexplore.ieee.org/xpl/login.jsp?tp=&arnumber=6268312&url=http%3A%2F%2Fieeexplore.ieee.org%2Fxpls%2Fabs_all.jsp%3Farnumber%3D6268312
- [25] L. Osborne, Apr. 2016, Reposit Power, private communication.
- [26] E. Twining and D. G. Holmes, “Grid current regulation of a three-phase voltage source inverter with an lcl input filter,” *IEEE Transactions on Power Electronics*, vol. 18, no. 3, pp. 888–895, May 2003.

- [27] D. Shepherd, "Integration of renewable energy onto the electricity grid," Master's thesis, University of New South Wales, Oct. 2012.
- [28] "Future power system security program - progress report," Australian Energy Market Operator, Tech. Rep., Aug. 2016. [Online]. Available: <http://www.aemo.com.au/Electricity/National-Electricity-Market-NEM/Security-and-reliability/-/media/823E457AEA5E43BE83DDD56767126BF2.ashx>
- [29] "Preliminary report – black system event in south australia on 28 september 2016," Australian Energy Market Operator, Tech. Rep., Oct. 2016. [Online]. Available: <http://www.aemo.com.au/Media-Centre/-/media/BE174B1732CB4B3ABB74BD507664B270.ashx>

Appendices

Appendix A Data Points For Frequency Deviations

Table 2 lists the data points which were used to generate the simple frequency deviation ramp in Section VII.1 on page 35. Table 3 lists the data points which were used to generate the realistic frequency deviation curve in Section VII.2 on page 40.

Table 2: Data points for simple frequency deviation.

Time (s)	Frequency (Hz)
5.0	50.00
12.5	50.75
17.5	50.75
25.0	50.00
32.5	50.00
40.0	49.25
45.0	49.25
52.5	50.00
57.5	50.00

Table 3: Data points for realistic frequency deviation.

Time (s)	frequency (Hz)
0.0	50.00
1.0	49.90
2.0	49.81
3.0	49.74
4.0	49.67
5.0	49.61
6.0	49.56
7.0	49.52
8.0	49.50
9.0	49.50
10.5	49.53
12.5	49.58
14.5	49.64
17.5	49.70
20.5	49.76
24.5	49.82
30.5	49.88
36.5	49.92
42.5	49.97
48.5	49.99
54.5	50.00

Appendix B Further Results

B.1 Realistic Over-frequency Deviation

Figure 26 shows the output power during a realistic over frequency deviation, for an inverter

- with droop control and inertia emulation both disabled;
- with droop control enabled and inertia emulation disabled; and
- with droop control and inertia emulation both enabled.

The over frequency deviation curve is the inverse of the under frequency curve shown in Table 3. The resulting power output approximately matches the inverse of power output during the under frequency event tested in Section VII.2 on page 40.

Figure 27 shows the output power of the inverter with both droop control and inertia emulation enabled, and compares it to an ideal generator. The experimental results are sufficiently close to the ideal curve.

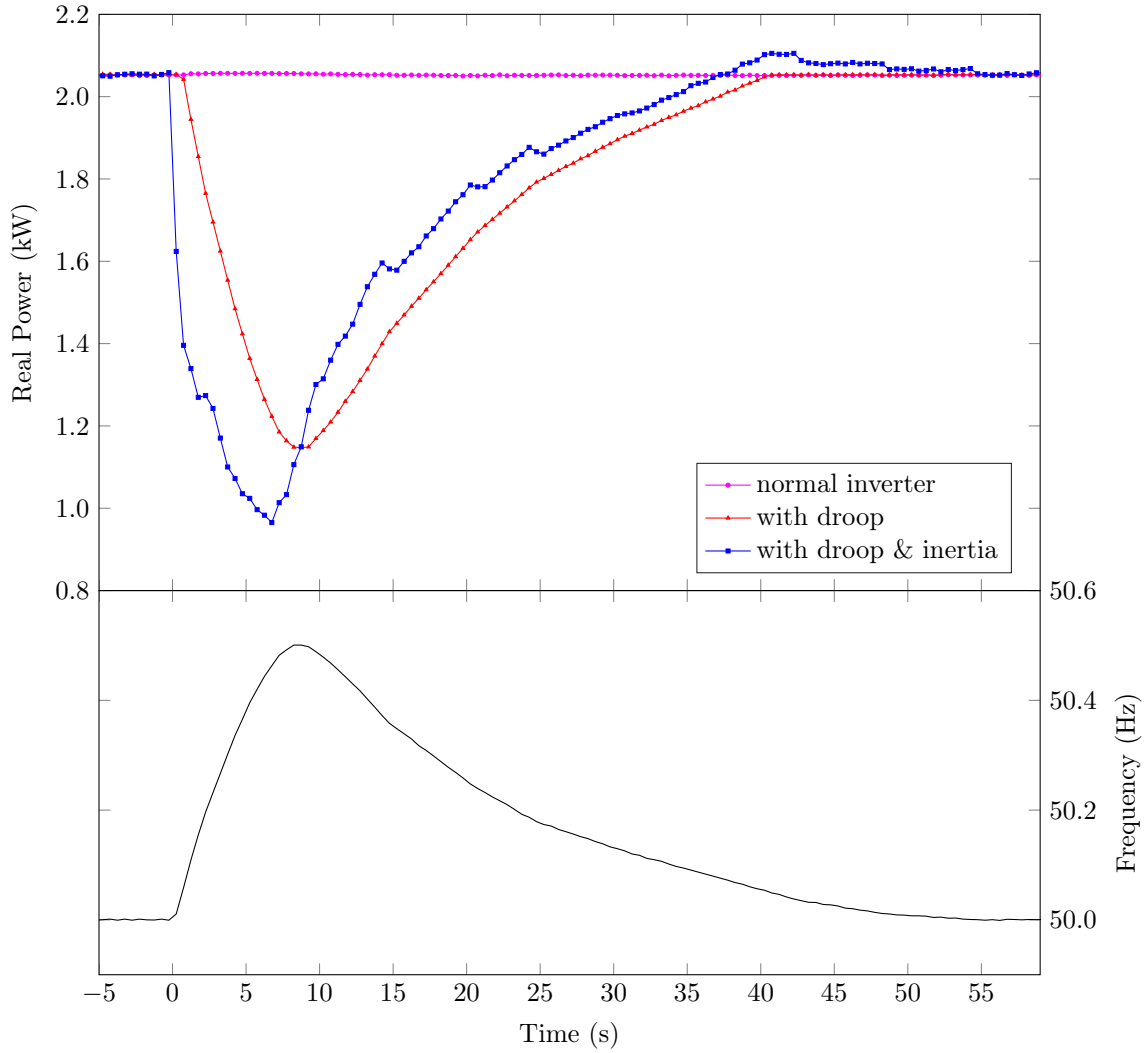


Figure 26: Experimental results showing the effect of droop and virtual inertia on output power (upper subplot) during a realistic over frequency deviation (lower subplot). A normal inverter (pink) produces a constant power output. Droop control (red) subtracts an amount proportional to the frequency from the nominal power output. Inertia emulation (blue) subtracts an amount equal to the derivative of frequency from the power output.

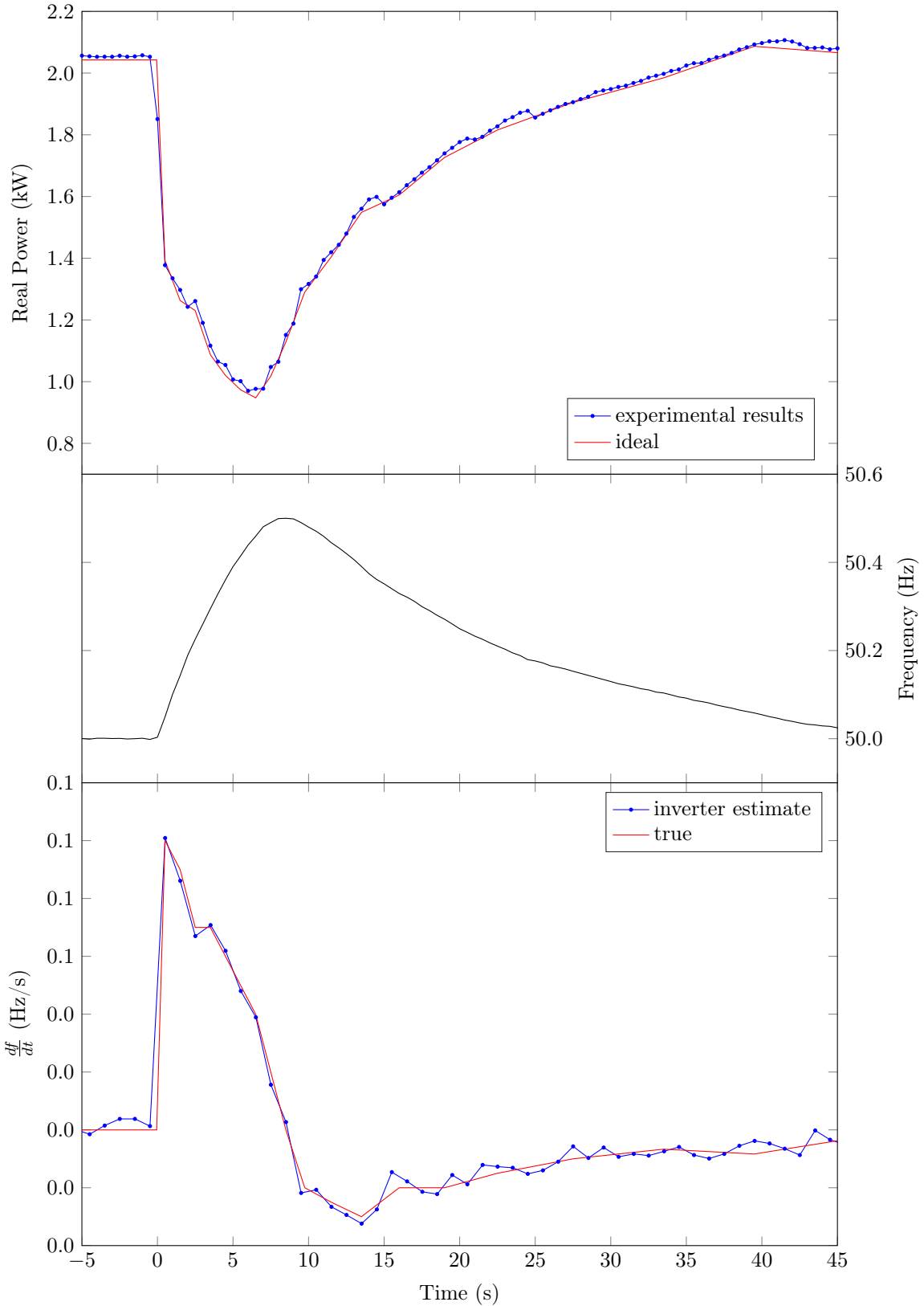


Figure 27: Experimental results showing the effect of droop and inertia emulation on output power during a realistic over frequency deviation. The top subplot compares the inverter power output to a conventional generator with droop control and real inertia. The inverter's estimate of frequency and its derivative is compared to the true value in the middle and bottom subplot respectively.

B.2 Saturation

Figure 28 shows an experimental test with a real power setpoint of 3.5 kW, and with both droop control and inertia emulation enabled. The target power exceeds the current rating of the inverter, so the control system saturates the output power. This is an inherent limitation of VSMs.

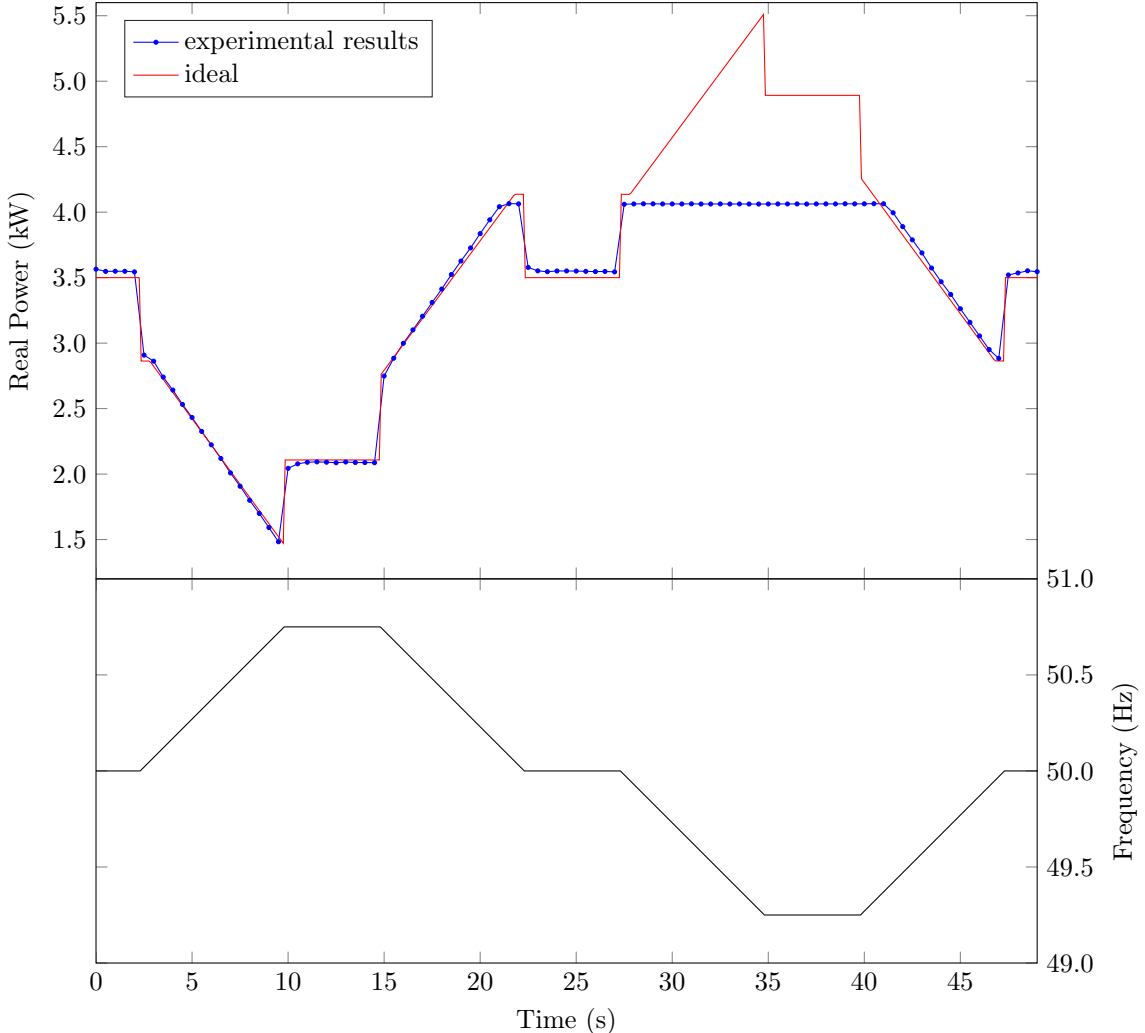


Figure 28: Demonstration of control system saturation. The output power and frequency are shown in the upper and lower subplots respectively. The high setpoint means that the target power exceeds the rating, so the control system saturates.